Dear Editor,

We wish to submit an article titled "Permeability Characterisation of Sedimentological Facies in the Bunter Sandstone Formation, Endurance CO_2 Storage Site, Offshore UK" as a preprint. The authors and their affiliations are listed below:

Shakhawat Hossain (s.hossain21@imperial.ac.uk)[1,2], Gary J. Hampson (g.j.hampson@imperial.ac.uk)[1], Carl Jacquemyn (c.jacquemyn@imperial.ac.uk)[1], Matthew D. Jackson (m.d.jackson@imperial.ac.uk)[1], Domenico Chiarella (Domenico.Chiarella@rhul.ac.uk)[3]

1. Department of Earth Science and Engineering, Imperial College London, London, SW7 2AZ, UK

2. Department of Geology, University of Dhaka, Dhaka 1000, Bangladesh

3. Department of Earth Sciences, Royal Holloway, University of London, Egham, Surrey, TW20 0EX, UK

The manuscript was originally submitted to the "International Journal of Greenhouse Gas Control" and went through review once. This is the revised manuscript that we submitted to the journal after addressing the reviewer's comments.

Best wishes,
Shakhawat Hossain
Postgraduate researcher
Imperial College London

Permeability Characterisation of Sedimentological Facies in the Bunter Sandstone Formation, Endurance CO_2 Storage Site, Offshore UK

Shakhawat Hossain[1,2], Gary J. Hampson[1], Carl Jacquemyn[1], Matthew D. Jackson[1], Domenico Chiarella[3]

1. Department of Earth Science and Engineering, Imperial College London, London, SW7 2AZ, UK

2. Department of Geology, University of Dhaka, Dhaka 1000, Bangladesh

3. Department of Earth Sciences, Royal Holloway, University of London, Egham, Surrey, TW20 0EX, UK

Table of Contents

Abstract

Permeability variations due to sedimentological heterogeneity are important in controlling CO_2 migration pathways, CO_2 plume dynamics, and stratigraphic, capillary and dissolution trapping of CO_2 in subsurface storage units and complexes. Thus, knowing these parameters is crucial to developing a CO_2 injection strategy that maximizes storage and trapping efficiency. In this study we analyzed the sedimentological and permeability heterogeneity of the Bunter Sandstone Formation at the Endurance CO_2 storage site, offshore UK, through integrated facies analysis, minipermeameter measurements, and thin section analysis. Detailed core logging and outcrop analysis were performed to identify facies and related heterogeneities. Twelve lithofacies have been identified in cores. By analyzing the stacking patterns of the facies, three facies associations and three architectural elements were identified in cores and outcrop analogues, respectively. Heterogeneities occur at all the scales ranging from mm-scale laminae to 10's m-scale architectural elements.

Permeability variations at outcrop and in core are closely related to sedimentological heterogeneities. Minipermeameter and core plug permeability data show up to three orders of magnitude variation across the facies. Cross-bedded (Sp, St, Sl, Spmc) and structureless (Sm) sandstones are the most permeable (4-5400 mD) facies, whereas pebbly conglomerates (Gmg) and laminated mudstones (Fl) are least permeable (0.18-89 mD) facies. Mottled and deformed sandstone (Smd) and crinkly laminated sandstone (Sc) have highly variable permeability (0.69-480 mD). Minipermeameter data reveal permeability varies by a factor of five at centimeter scale within planar cross-bedded (Sp), trough cross-bedded (St) and planar bedded sandstone (Sh) sandstone facies, while planar cross-bedded sandstone with mud clasts along foresets (Spmc) exhibit permeability variation up to a factor of four. Petrographic analysis of thin sections shows that these permeability variations are related to changes in grain size, clay content, and distribution of dolomite cements.

1 Introduction

Anthropogenic emissions of carbon dioxide (CO_2) have increased by 36% over the last 300 years and are considered the primary cause of climate change (Jones et al., 2023). To avoid the most severe consequences of climate change, atmospheric warming needs to be kept below 1.5^{o}C (Hoegh-Guldberg et al., 2018). Large scale geological storage of CO_2 in the subsurface has been proposed as a potential mitigating option to stabilize and diminish human-induced CO_2 emissions. This method depends on securely storing significant volumes of CO_2 underground in subsurface saline formations and depleted hydrocarbon reservoirs. The heterogeneous nature of geological formations is a crucial control how injected CO_2 moves and is contained (Trevisan et al., 2015). This complexity deeply influences the efficacy of dissolution (Farajzadeh et al., 2009; Agartan et al., 2015) and capillary trapping (Bryant et al., 2008; Trevisan et al., 2015) mechanisms. Thus, it is critical to understand geological heterogeneities and their impact on permeability in these geological formations. Understanding these factors are essential for unlocking the full potential of geological CO_2 storage in mitigating global carbon emissions. This study investigates the relationship between geological heterogeneity and permeability variations and considers their impact on CO_2 movement, storage and trapping. The Bunter Sandstone Formation is the storage unit in the Endurance CO_2 storage site – the first of its kind in the UK (Gluyas & Bagudu, 2020). Regional analysis of the Bunter Sandstone Formation utilizing petrophysical and seismic data suggests that reservoir properties are favourable for CO_2 injection, although the unit contains extensive mudstone layers and cemented intervals (Hollinsworth et al., 2024). The findings of this study will be helpful to understand the effects of small-scale variations in lithostratigraphically equivalent units (e.g., Buntsandstein in Germany and the Netherlands; (Arts et al., 2012) and in fluvial deposits in other parts of the world.

Upon injection, geological CO_2 storage is controlled by four trapping mechanisms, namely stratigraphic trapping, residual trapping, dissolution, and mineralization (Bachu & Adams, 2003). Fluid flow near the injection well bore is dominated by viscous forces, but as the distance from the injection well increases, capillary and buoyancy forces take over (Petrovskyy et al., 2023). Therefore, most of the storage reservoir in which CO_2 migration will take place will be dominated by capillary and buoyancy forces. It has been observed that sedimentological heterogeneity has a significant impact on multiphase flow dynamics in parts of the reservoir where capillary and buoyancy flow regimes dominate (Li & Benson, 2015).

The most important reservoir properties that control CO_2 migration and storage are effective porosity and permeability (Kovscek, 2002). These properties are controlled by the organization of sedimentological and structural heterogeneities within the reservoir. Different sedimentological facies exhibit varying degrees of permeability, which affects the efficiency of CO_2 injection and storage. Understanding the relationships between facies types and permeability variations therefore helps to constrain CO_2 migration pathways, plume dispersal and estimates of CO_2 storage capacity.

Many studies have been conducted on permeability variations associated with heterogeneity in different geological settings and deposits (Stalkup & Ebanks, 1986; Prosser et al., 1995; Ringrose et al., 1999; Possemiers et al., 2012). The main purpose of these studies was to understand their impact on hydrocarbon recovery efficiency (Lewis, 1988; Honarpour & Saad, 1994; Honarpour et al., 1995; Chen et al., 1999; Ringrose et al., 1999; Stephen et al., 2001; Rashid et al., 2012; Pantou, 2014; Gao & Li, 2016) and groundwater flow through aquifers (Freeze & Witherspoon, 1967; Cheng, 1984; Neuzil, 1986; Keller et al., 1988; Gotkowitz, 1993; Huysmans et al., 2008). These studies show that permeability heterogeneity occurs at different scales and they are strongly influenced by sedimentary architectures and clay contents, especially in high porosity sandstone units (Prosser et al., 1995; Ringrose et al., 1999; Possemiers et al., 2012). However, only a few studies have been conducted to understand the impact of heterogeneities on CO_2 migration in CO_2 storage reservoirs (Ambrose et al., 2008; Krevor et al., 2011; Trevisan et al., 2014; Krevor et al., 2015; Li & Benson, 2015; Trevisan et al., 2015; Gershenzon et al., 2017; Krishnamurthy et al., 2017; Trevisan et al., 2017; Krishnamurthy et al., 2022; Alshakri et al., 2023). Core flooding experiments undertaken in these studies primarily aim to understand the capillary trapping at the pore scale, but understanding how these effects propagate into larger scales is still a challenge. Thus, it is imperative to identify permeability heterogeneities at different length scales and to evaluate their effect on CO_2 trapping in order to apply core-scale findings at the storage unit scale robustly.

Probe permeameter data has been effective in characterising small-scale permeability variations related to sedimentological heterogeneity (Corbett et al., 1992; Honarpour & Saad, 1994; Ringrose et al., 2005; Huysmans et al., 2008). The non-destructive nature of the measurement allows collection of high-resolution data from the facies of interest. Minipermeameter data from the Sherwood Sandstone Group and equivalent Bunter Sandstone Formation have been previously collected from outcrops (McKinley et al., 2011) and cores (Weatherford, 2015), but not placed in the context of a sedimentological facies scheme, which limits the degree to which variability in permeability values can be predicted.

The aims of this paper are: (1) to identify and interpret variability in sedimentary facies in cores and analogous outcrops of the Bunter Sandstone Formation, and (2) to investigate the relationships between sedimentological facies, related heterogeneity and permeability variation in the Bunter Sandstone Formation.

2 Geological context

The Endurance CO_2 storage site is defined by a four-way dip closure that spans Blocks 42/25 and 43/21 in the UK sector of the North Sea, 60 miles east of the coast of Northeast England (Fig. 1). This closure is approximately 22 kilometers long, 8 km wide, and more than 200 meters high (Gluyas & Bagudu, 2020).

The Early Triassic Bunter Sandstone Formation is the targeted storage unit in the Endurance CO_2 storage site. The reservoir's crest is roughly 1020 m below the seabed, and the four-way closure is penetrated by three wells above the spill point (Fig.1B). The lithological characteristics and stratigraphic position of this formation and stratigraphic equivalents make it a key target for hydrocarbon exploration (e.g., Wytch Farm oil field), groundwater resources (onshore) and CO_2 storage (e.g., Southern North Sea and Liverpool Bay). This formation and its lithostratigraphic equivalents are widely distributed across Western and Central Europe, including large parts of Germany, France, the Netherlands and the United Kingdom. The Bunter Sandstone Formation is equivalent to the Sherwood Sandstone Group of the onshore UK, suggesting regional continuity of deposition (Medici et al., 2015).

The Bunter Sandstone Formation is overlain by the Middle to Late Triassic, evaporate-bearing Haisborough Group (equivalent to the Mercia Mudstone Group, onshore UK), which serves as a seal (Cameron et al., 1992). The Bunter Sandstone Formation unit was deposited in a continental setting, featuring a complex interplay of fluvial, aeolian, and lacustrine environments. The Formation reflects a time when most part of the continental Europe was characterized by arid to semi-arid conditions, with vast desert dune fields and ephemeral river systems (Ziegler, 1982).

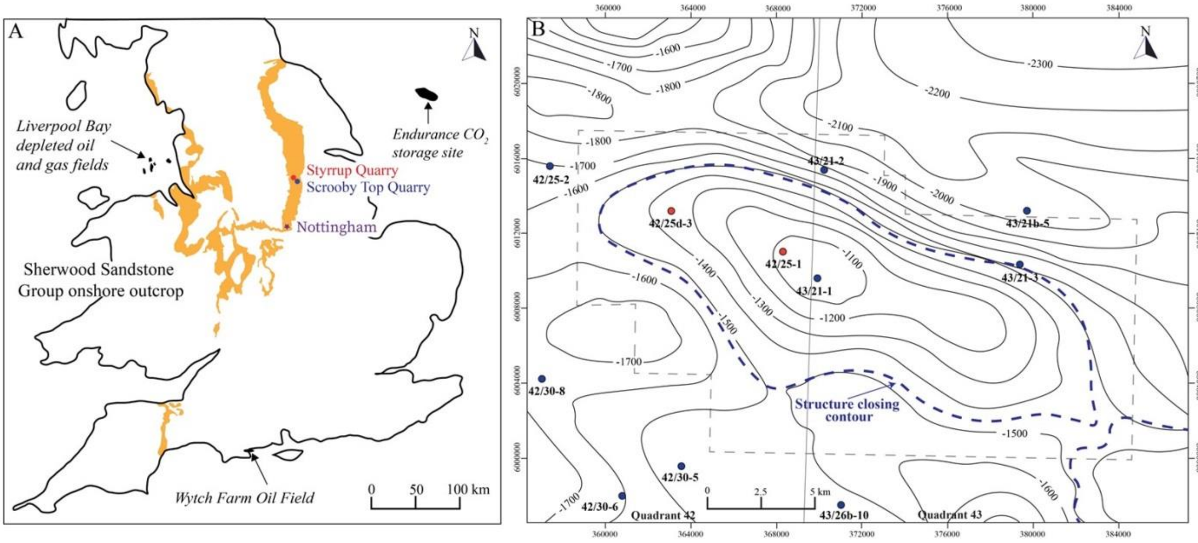

Figure 1: A) Map showing the distribution of Sherwood Sandstone Group outcrops (orange) in the onshore UK and occurrence in subsurface reservoirs (black). Red and blue circle show the location of the Styrrup Quarry and Two Oaks Quarry and Nottingham outcrops. B) Depth structure map of the Endurance CO_2 storage site and wells drilled within the structural closure of the site (modified after (Gluyas & Bagudu, 2020). Cores from two wells highlighted in red were studied for facies analysis.

3 Data and Methodology

The study integrates detailed facies analysis of core and outcrop data, core plug and minipermeameter permeability measurements, and thin sections of selected core and outcrop samples.

3.1 Facies analysis

3.1.1 Core

Core data from wells 42/25-1 and 42/25d-3 covering an interval of 10 and 163 meters (Fig. 4) respectively were studied to construct a lithofacies scheme that characterises small-scale sedimentological heterogeneity. Detailed sedimentological logging of the cores was performed for the purpose of facies analysis. The overall quality of core from well 42/25d-3 is very good, while core from well 42/25-1 is poor in quality. Cores from the well 42-25-1 are mostly broken therefore sedimentary structures were not readily identifiable, whereas cores from well 42-25d-3 are new and well preserved.

3.1.2 Outcrop analogue

Outcrop analogues are key to understand facies distributions and the dimensions, geometry and distribution of heterogeneities at inter-well scale and constrain the lateral extent of these facies.

The Sherwood Sandstone Group, which is lithostratigraphically equivalent to the Bunter Sandstone Formation, is exposed in several quarries (e.g., Styrrup Quarry, Scrooby Top Quarry, Two Oaks Quarry, Breedon Quarry) and man-made faces (e.g., Park Tunnel, Nottingham Castle) in Nottinghamshire, eastern UK. In the well-preserved Styrrup Quarry (Fig.1A) exposure, we collected data to supplement a previously published architectural panel with lateral dimensions of 110 m and 30 m in NNW-SSE and ENE-WSW orientations, respectively (Wakefield et al., 2015). The height of the quarry faces is 8 m. The architectural panel shows the different architectural elements exposed on the quarry faces and their relationship with each other. We apply the core-based facies scheme to this outcrop face, and also describe four small (c. 1 m) measured sections to characterize individual facies and collect minipermeameter data and samples for thin-sections. There is a dearth of natural outcrops of the Bunter Sandstone Formation in the eastern UK, hence the preserved outcrop in Styrrup Quarry has been considered as an analogue for the Bunter Sandstone Formation in the Southern North Sea by many authors (McKinley et al., 2011; McKinley et al., 2013; Wakefield et al., 2015). This outcrop allows identification of sedimentary facies and architectural elements in detail, even though it is far from the Endurance CO_2 storage site (Fig. 1A). We have also been to some well exposed outcrops in the Park Tunnel and Nottingham Castle in the Nottingham city centre.

3.2 Minipermeametry measurements

Permeability measurements for all the lithofacies identified in the core and three lithofacies described in the outcrop were taken using a portable hand-held air permeameter (Tiny Perm 3). Permeability readings were taken using a 10 cm large grid for a total of 20 measurements per facies. For facies containing planar laminae, measurements were collected on an orthogonal grid. For lithofacies with inclined laminae, such as foreset in planar and trough cross bedded sandstone, measurements were taken along the inclined laminae. It was difficult to measure permeability where the cores were broken, because fractures can significantly impact permeability measurements. Outcrop faces are highly weathered, and there were few smooth surfaces against which measurements could be taken.

3.3 Thin section Petrography

Thin section petrography was performed to identify the causes of permeability variations between and within lithofacies. Ten thin sections were prepared for selected lithofacies in core and three from selected lithofacies at outcrop. Thin sections were studied under petrographic microscope to characterise texture and mineralogy, for comparison with variations in permeability.

4 Results

4.1 Core and outcrop facies analysis

In the outcrops examined for this study, the Sherwood Sandstone is composed of medium to fine grained sandstone with pebbles, whereas the studied cores contain additional mudstone-bearing lithologies. In total, 13 lithofacies have been identified. Descriptions and interpretations of the lithofacies are summarized in Table 1. Matrix-supported conglomerate (Gmg), planar cross-bedded sandstone (Sp), planar cross-bedded sandstone with clasts along foresets (Sph), interbedded siltstone and sandstone (Sss), parallel-laminated sandstone (Sh), structureless sandstone (Sm), trough cross laminated sandstone (St), and laminated mudstone (Fl) are common in both the cores and outcrop (Figs. 2, 3). In addition, low angle cross bedded sandstone (Sl), mottled and deformed sandstone (Smd), crinkly laminated sandstone (Sc), and rippled sandstone (Sr) are identified in core from well 42/25d-3 (Fig. 5).

Table 1: Descriptions and interpretations of lithofacies in outcrop and core.

Lithofacies	Description	Interpretation	Permeability (mD)
Matrix-supported conglomerate (Gmg)	Conglomerates and sandstone; fine to coarse grained sand matrix with grey mudstone clasts that are 10–40 mm in diameter. Clasts are sub-rounded to sub-angular.	Intraclasts record the localised reworking of mudstone beds with clasts derived either via erosion from the base of channels or from bank collapse at channel margins.	0.7-89
Planar cross-bedded sandstone (Sp)	Fine to medium-grained, moderately sorted sandstone arranged in sets of cross beds. Individual cross-sets are 10-12	Downstream migration and deposition of straight-crested dunes under low flow regime conditions.	9.5 -5350

	cm thick. Both the topset and the bottomset are horizontal to slightly inclined. Foresets are inclined at 17-23˚. Foreset consists of alternating clay-poor and clay-rich laminae.		
Low angle cross-bedded sandstone (Sl)	Fine to medium-grained, moderately sorted cross bedded sandstone. Individual set thickness is around 20-30 cm. Foresets are inclined at <15^0	Downstream migration and deposition of straight-crested dunes under low flow regime conditions.	35-1673
Trough cross-bedded sandstone (St)	Medium to fine grained cross bedded sandstone. Individual sets are 40-80 cm thick and they consist of multiple sets.	Downstream migration of sinuous-crested dunes under lower flow regime conditions.	13 – 2813
Trough cross-laminated sandstone (St1)	Multiple sets of fine to medium-grained, moderately sorted trough cross-laminated sandstone. Individual sets are 10-15cm thick, and cosets are 0.6-1 m thick. Dark coloured clay-rich laminae are present along the troughs. The basal surfaces are commonly erosional.	Downstream migration and deposition of sinuous-crested ripples under lower flow regime conditions.	35-1673
Planar cross-bedded sandstone with mud clasts (Spmc)	Well-sorted, fine to medium grained, cross-bedded sandstone with mud clasts along foresets. Clasts are rounded and 20-40 mm in diameter.	Downstream migration and deposition of straight-crested dunes under lower flow regime conditions. Mud clasts represents broken fragments of previously deposited (Fl) facies which have been reworked into the channel.	4-3853
Parallel-laminated sandstone (Sh)	Fine-grained, well-sorted sandstone containing planar-parallel lamination. Clay-rich laminae are present. Thickness of this unit ranges from 05-1.5 m.	Migration and deposition of sandy bedforms under upper flow regime conditions.	7.2-2468
Structureless sandstone (Sm)	Fine to medium grained, moderately to well sorted sandstone with erosional base. Units are 30-50cm thick and often overlie mudstone units.	Deposition from laminar, high density sandy flows.	9.5 -5350
Fine sandstone and siltstone (Sss)	Siltstone with subordinate thin (20-50 cm) beds of fine-grained sandstone. Sandstones are typically cross-bedded. Units contain abundant sand-filled desiccation cracks.	Deposition during falling flow stage, and subsequent subaerial exposure.	1.14-588
Laminated mudstone (Fl)	Laminated, dark brown mudstone with rare siltstone laminae. Units are typically 10-20 cm thick, but rarely up to 50 cm thick.	Deposition from suspension in overbank areas and abandoned channels.	0.18-2.92

Mottled and deformed sandstone (Smd)	Fine grained sandstone with deformations in the form of harmonic and disharmonic folds, antiform shapes, and subvertical pipes.	Deformation due to escape of overpressured water.	2.8-480
Crinkly laminated sandstone (Sc)	Thin units (10-20 cm) of siltstones and very fine-grained sandstones with irregular to highly diffuse, crinkly and variably continuous lamination.	Adhesion ripples and warts deposited on a damp substrate.	0.69-180
Rippled sandstone (Sr)	Fine grained, moderately sorted sandstone containing symmetrical cross-lamination in beds 10-20 cm thick.	Downstream migration and deposition of current ripples under lower flow regime conditions. Symmetrical ripple forms record wave reworking.	8-160

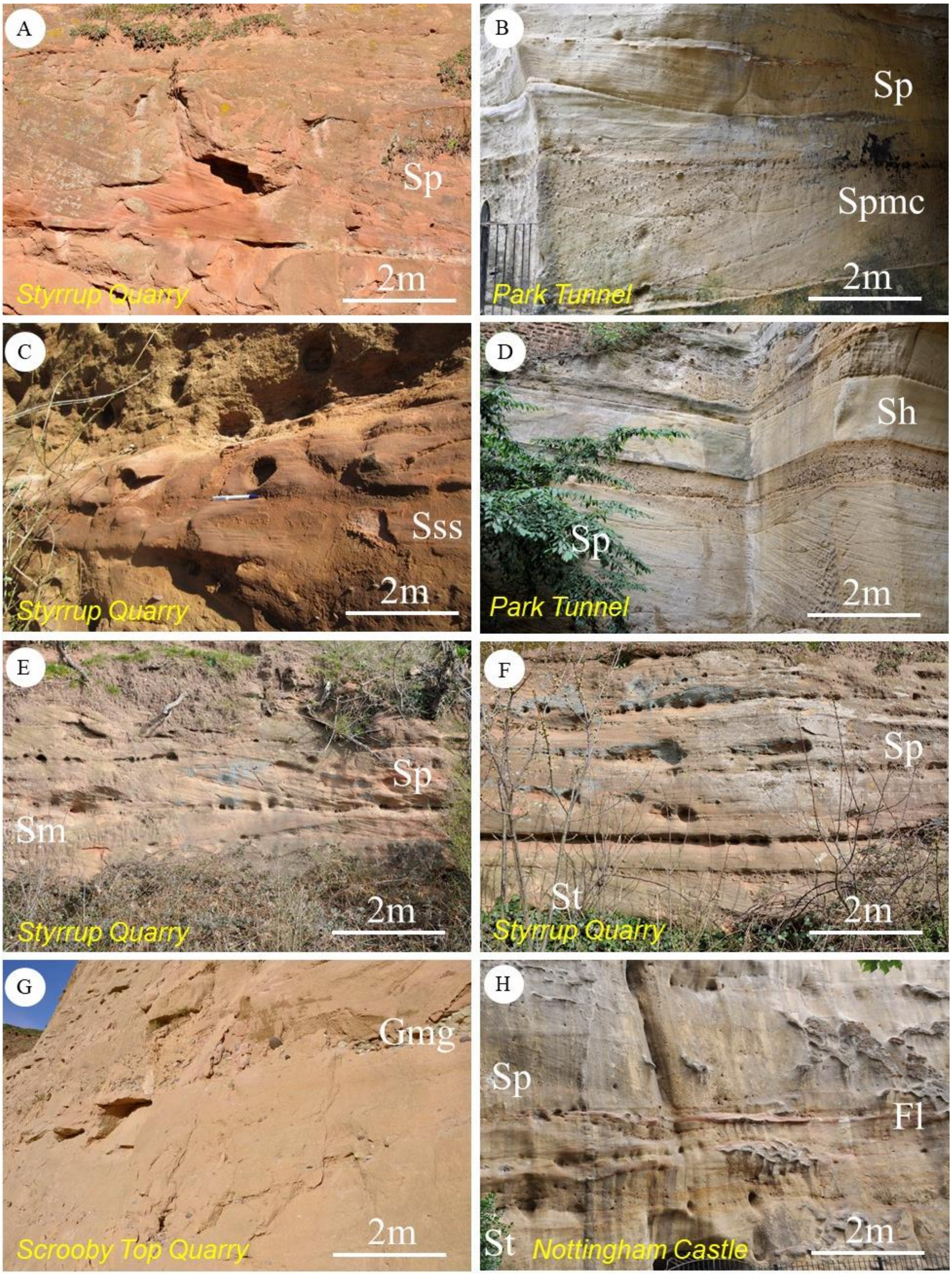

Figure 2: Lithofacies identified in quarry-face and man-made outcrops (Fig. 1A): A) planar cross-bedded sandstone (Sp); B) planar cross-bedded sandstone with mud clasts (Spmc); C) Fine sandstone and siltstone (Sss); D) parallel-laminated sandstone (Sh); E) structureless sandstone (Sm); F) trough cross-bedded sandstone (St); G) matrix-supported conglomerate (Gmg); and H) laminated mudstone (Fl).

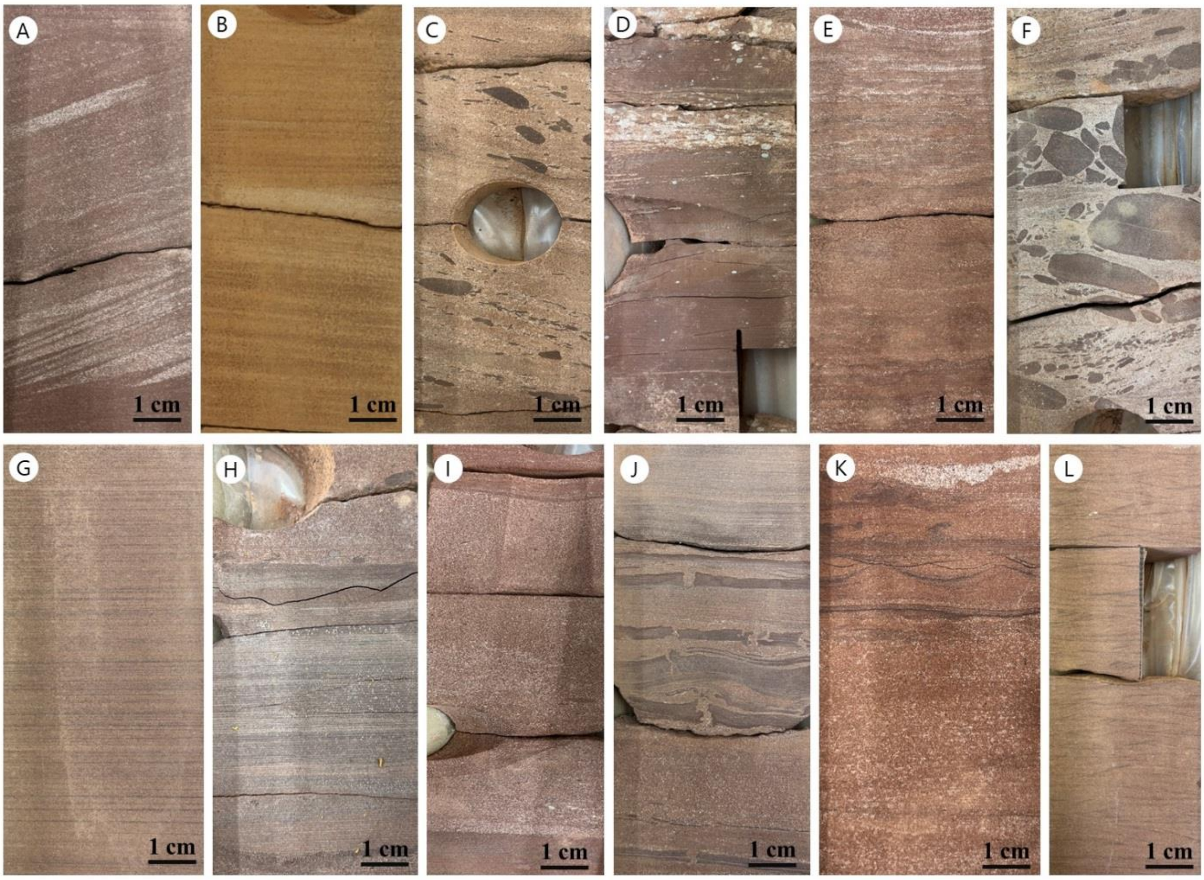

Figure 3: Lithofacies identified in the cores of well 42/25d-3: A) planar cross-bedded sandstone (Sp); B) low-angle cross-bedded sandstone (Sl); C) planar cross-bedded sandstone with mud clasts (Spmc); D) laminated mudstone (Fl); E) crinkly laminated sandstone (Sc); (F) matrix-supported conglomerate (Gmg); G) parallel-laminated sandstone (Sh); (H) Fine sandstone and siltstone (Sss); I) structureless sandstone (Sm); J) mottled and deformed sandstone (Smd); K) rippled sandstone (Sr); and L) trough cross-laminated sandstone (St1).

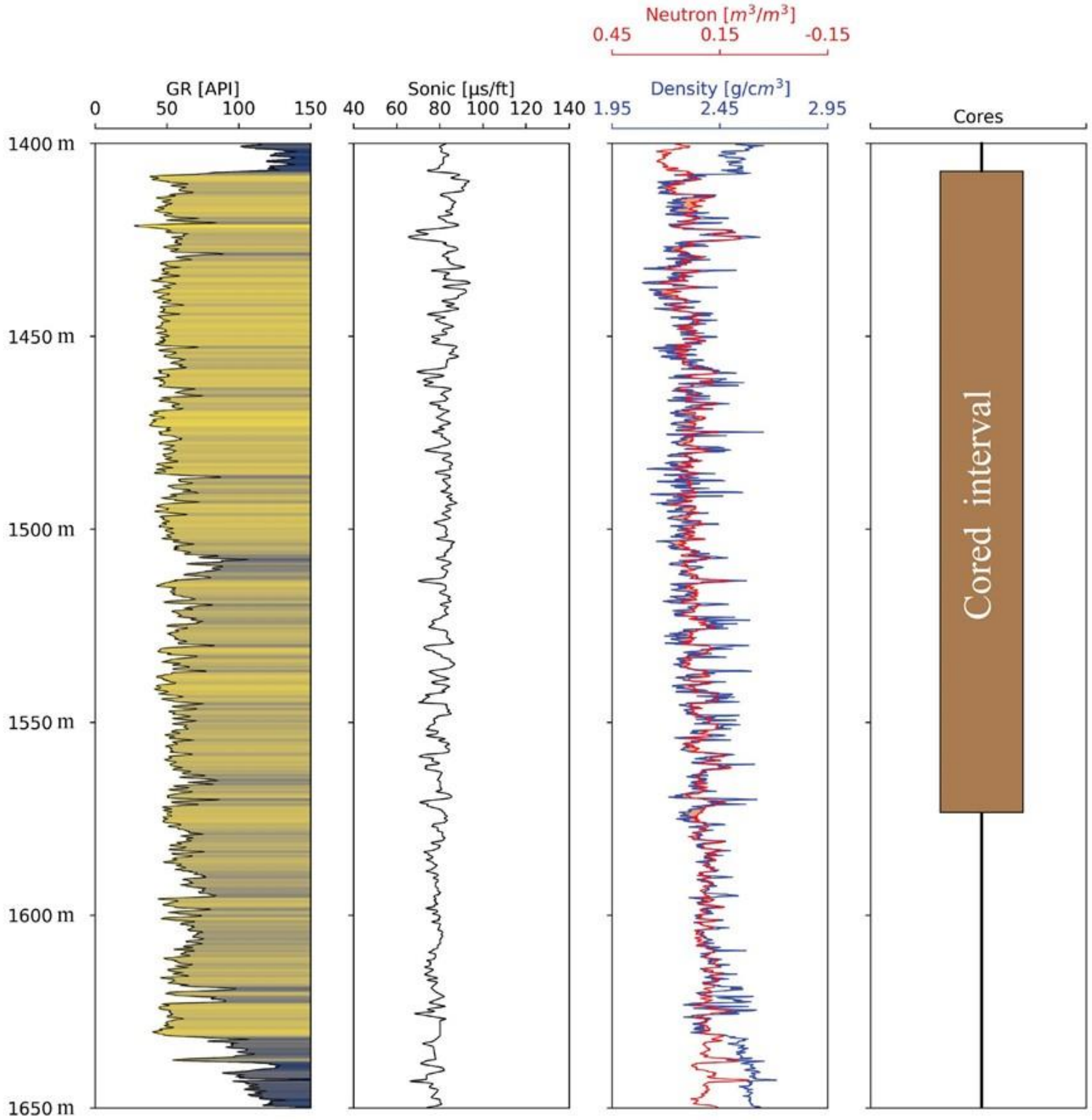

Figure 4: Geophysical logs of well 42/25d-3 and the cored interval (c. 163 m).

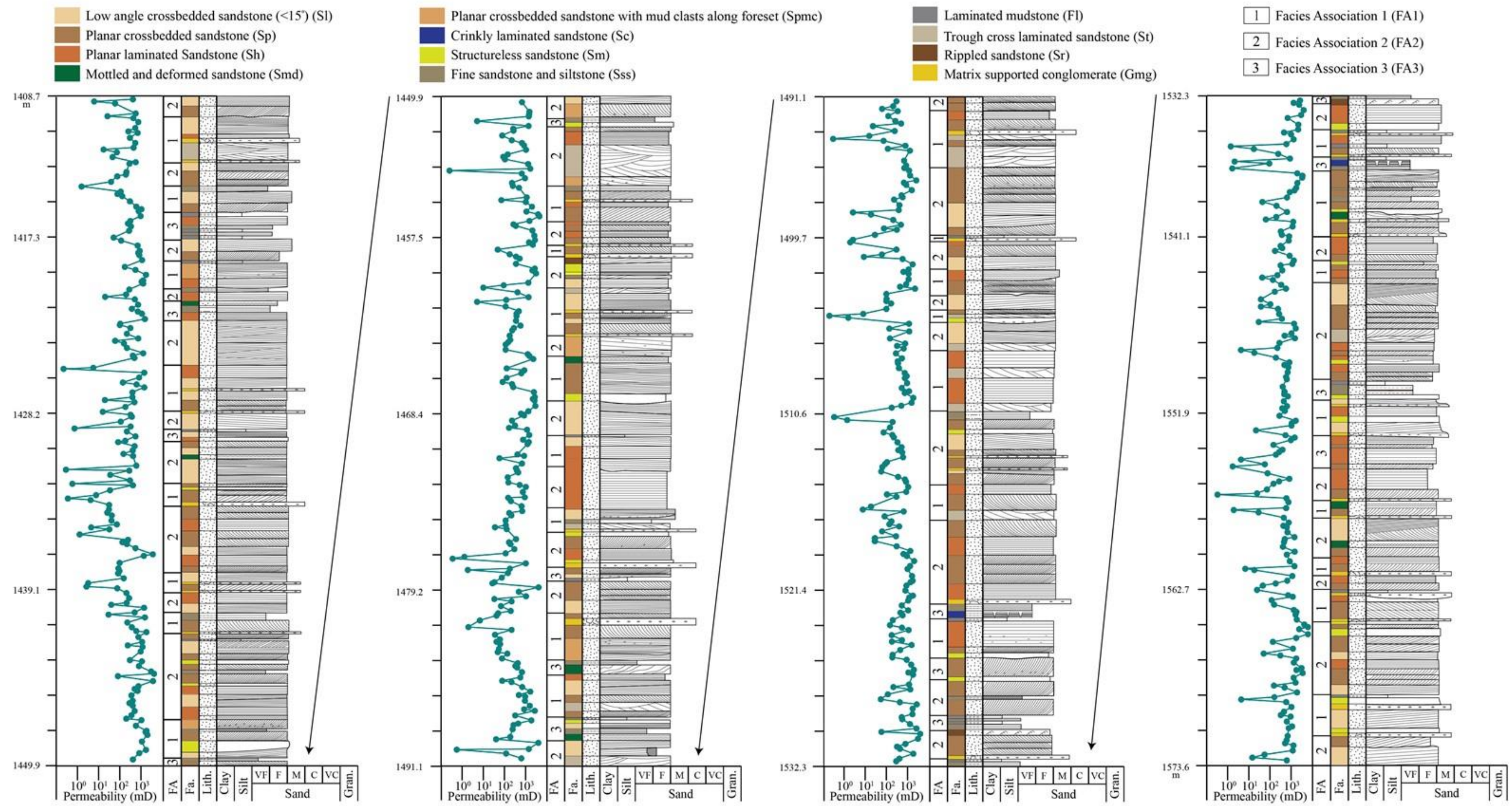

Figure 5: Sedimentological log through core in well 42/25d-3, illustrating the vertical stacking of lithofacies to form facies associations and the corresponding core plug permeability.

4.2 Facies associations

Lithofacies recording depositional processes recur in associations that characterise depositional environments. Facies associations are integrated with outcrop observations to constrain the dimensions and geometry of architectural elements. Three facies association have been identified, as summarized below.

4.2.1 FA1: Channel-fill deposits

Description: Facies Association 1 consists of the following lithofacies arranged in units 2-3 m thick: matrix-supported conglomerate (Gmg), planar cross-bedded sandstone (Sp), planar cross-bedded sandstone with mudclasts (Spmc), parallel-laminated sandstone (Sh), interbedded sandstone and siltstone (Sss), crinkly laminated sandstone (Sc) and laminated mudstone (Fl) (Fig. 6). In an idealized vertical succession through the facies association, matrix-supported conglomerate (Gmg) at the base is overlain by planar cross-bedded sandstone (Sp, Spmc) in which cross-set thickness and mudclast abundance decrease upwards, and then parallel-laminated sandstone (Sh) and the unit is capped by interbedded sandstone and siltstone (Sss) and laminated mudstone (Fl). A decrease in grain size is also observed from base to top of this idealized succession. The basal conglomerate unit is not present in the all units of the facies association. In some units, crinkly laminated sandstone (Sc) caps successions of the facies association. At outcrop, this facies association has a channelized or lenticular geometry and have a facies association consisting of matrix-supported conglomerate (Gmg), trough cross-bedded sandstone (St), planar cross-bedded sandstone with mudclasts (Spmc), and structureless sandstone (Sm) (Fig. 6). Units of the facies association show a crude fining-upward trend and are typically 2-4m thick and can be traced laterally for up to 25m. Palaeocurrent data measured from the cross beds in the Styrrup Quarry outcrops have an azimuth of 162˚.

Interpretation: Facies Association 1 is interpreted to represent channel-fill deposits (Gibling, 2006). Basal conglomerate (Gmg) is associated with the initial channel scouring and overlying cross-bedded sandstone (Sp, Spmc) represents migration of dunes within the channel. The upward thinning of cross-beds represents an upward decrease in dune height due to shallowing of water depth. Where cross-bedded sandstone (Sp, Spmc) is overlain by parallel-laminated sandstone (Sh), this transition records a shift from lower to upper flow regime conditions. Interbedded sandstones and siltstones (Sss) and laminated mudstone (Fl) at top of this association formed during the falling stage and cessation of flow in the channel, while crinkly laminated sandstone (Sc) may have formed when wind blew over the wet surface of the partially infilled channel (Porada et al., 2008). Mudclasts in this association were not transported a long distance, as indicated by their relatively large size and subrounded-to-angular shape, and may have been eroded from fine-grained overbank deposits. Palaeocurrents in the Styrrup Quarry outcrops are parallel to the regional flow direction of Sherwood Sandstone palaeo-rivers (Wakefield et al., 2015).

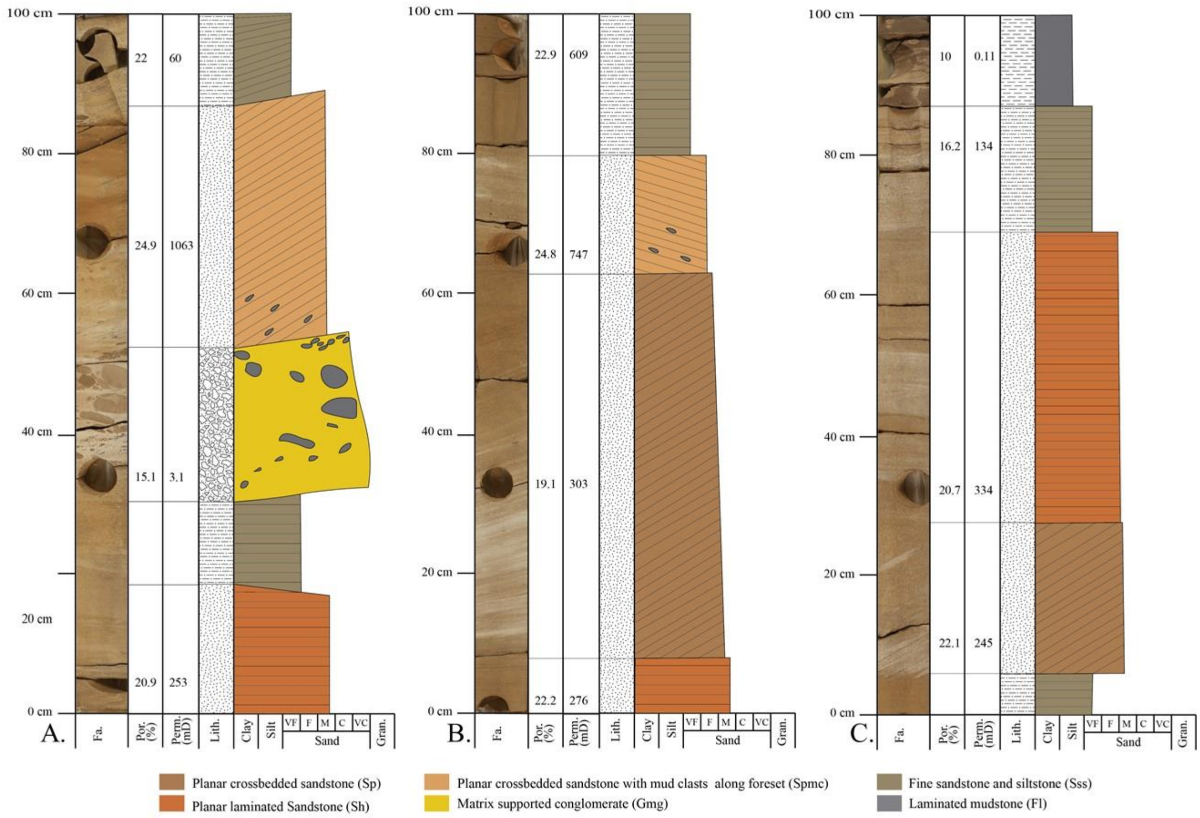

Figure 6: Core photos and sedimentological logs through core in well 42/25d-3 with core plug porosity and permeability, illustrating channel-fill deposits (Facies Association 1). The core photos are from the following depths: A) 1478.3-1479.3 m; B) 1514.8-1515.8 m; and C) 1570.6-1571.6 m.

4.2.2 FA2: Lateral- and downstream-accreting bars

Description: Facies Association 2 consists of the following lithofacies arranged in units 1-4 m thick: low-angle cross-bedded sandstone (Sl), planar cross bedded sandstone (Sp), trough cross-laminated sandstone (St), parallel-laminated sandstone (Sh), and laminated mudstone (Fl) (Fig. 7). An idealized succession through the facies association consists of low-angle cross-bedded sandstone (Sl) at the base overlain successively by planar cross bedded sandstone (Sp), trough cross laminated sandstone (St1), parallel-laminated sandstone (Sh) and laminated mudstone (Fl) towards the top. This idealized succession is rare. Instead, alternating layers of parallel-laminated sandstone and trough cross-laminated sandstone (St1) are the most abundant lithofacies successions. The lack of dipmeter data makes it difficult to estimate paleocurrent directions. However, similar facies associations have been identified at outcrop. The cross-bedded facies (Sp, Spmc, St, Sl) constitute more than 80% of the association, while the rest is usually made up of Sh, Sr and Sss. Units of the facies association have a lensoidal shape and the upper surface is convex down in some examples (Fig. 9). The thickness of this association in the outcrop ranges from 2-4.5 m. Palaeocurrent data measured from the cross beds in the outcrop show two dominant directions which are 351^{o} and 173^{o} (Wakefield et al., 2015).

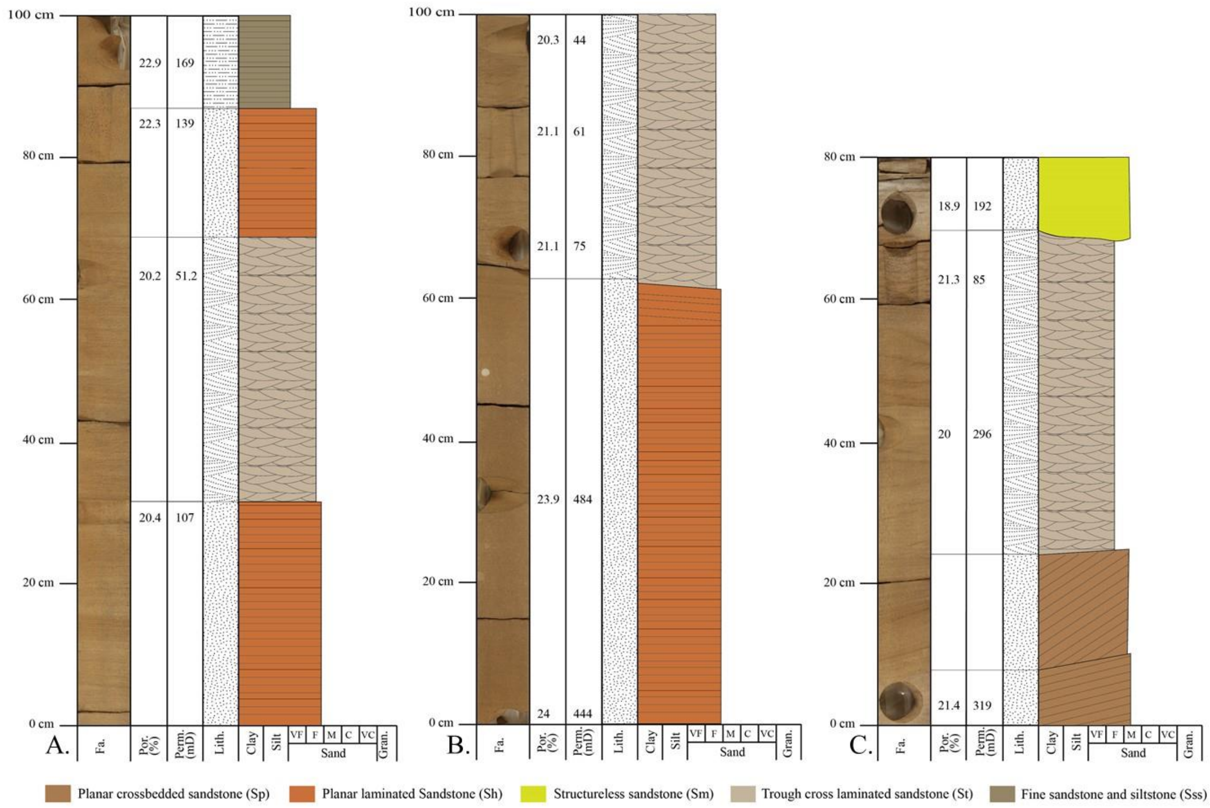

Figure 7: Core photos and sedimentological logs through core in well 42/25d-3 with core plug porosity and permeability, illustrating lateral- and downstream-accreting bar deposits (facies association 2). The core photos are from the following depths: A) 1511.2-1512.2 m); B) 1509.3-1510.3 m; and C) 1565.1-1566.1 m.

Interpretation: Facies Association 2 is interpreted to represent lateral- and downstream-accreted bars (Miall, 1977; Ghazi & Mountney, 2009; Grenfell, 2012). Association dominated by low-angle cross-bedded sandstone (Sl) is common in ephemeral stream deposits, and is typically associated with the lateral migration (Picard & High, 1973).

Inclined bedding in the Sl dominated intervals show a direction perpendicular to palaeocurrent directions, supporting the interpretation of lateral bar accretion. Inclined bedding in other intervals is parallel to palaeocurrent directions, indicating downstream bar accretion. The presence of parallel-laminated sandstone (Sh) on top of cross-bedded sandstone (Sl, St1) indicates a change from lower to upper flow regime, possibly due to decrease in water depth. The convex down shape of the bounding cosets of cross-beds preserves bar geometry.

4.2.3 FA3: Overbank deposits

Description: Facies association 3 consists of the following lithofacies arranged in units 0.2-1.8 m thick: parallel-laminated sandstone (Sh), interbedded sandstone and siltstone (Sss) and laminated mudstone (Fl). Cross-bedded sandstones (St1, Sr) also occur as minor constituents (Fig. 8). This facies association differs from the others in that erosional surfaces are absent. Contacts between the facies are gradational. The most common facies in this association are interbedded sandstone and siltstone (Sss) and mudstone (Fl).

Interpretation: The prevalence of parallel-laminated sandstone (Sh), interbedded sandstone and siltstone (Sss) and laminated mudstone (Fl) is suggestive of deposition on a sandy floodplain (Fisher et al., 2007; Lewin & Ashworth, 2014) while the absence of matrix-supported conglomerate (Gmg) implies the absence of channelised flow. Parallel-laminated sandstone units (Sh) are interpreted as proximal floodplain deposits that formed during non-channelized flows during flood events. Cross-laminated sandstone and rippled sandstone are interpreted as intermediate floodplain deposits, while interbedded sandstone and siltstone (Sss) and laminated mudstone (Fl) are interpreted as distal floodplain deposits.

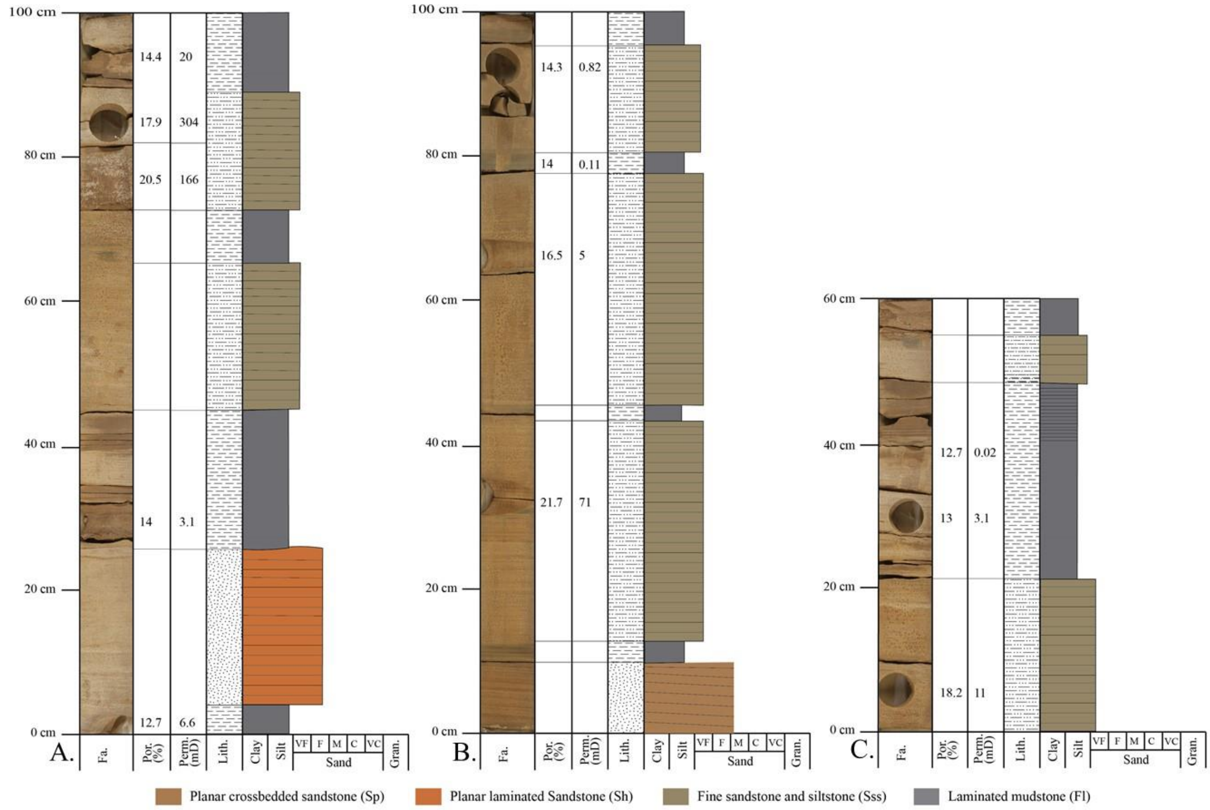

Figure 8: Core photos and sedimentological logs through core in well 42/25d-3 with core plug porosity and permeability, illustrating overbank deposits (facies association 3). The core photos are from the following depths: A) 1542.3-1543.3 m; B) 1518.5-1519.5 m; and C) 1548.7-1549.7 m.

4.3 Architectural element analysis

Five types of architectural elements were documented in the Styrrup Quarry outcrop by (Wakefield et al., 2015), based on their lithofacies composition, the geometry and character of their bounding surfaces, and their paleocurrent orientations (Table 2). Similar architectural elements have been documented in studies of the Sherwood Sandstone Group and Bunter Sandstone Formation in other outcrops (e.g., (Medici et al., 2015). Figure 8 shows a modification of the architectural panel constructed by (Wakefield et al., 2015) that has been adapted to match the lithofacies scheme summarised in Table 1. Architectural elements documented at outcrop are compared to facies associations with similar constituent facies in core. Several architectural elements could not be differentiated in core (e.g., lateral- and downstream-accretion elements), and are thus grouped together. The five architectural elements identified by Wakefield et. al. (2015) have been regrouped into three architectural elements to match the facies associations identified in the cores (Fig. 9). Detailed measured sections through selected facies are shown in Figure 9.

Architectural elements are showing the lateral extent of the facies associations and the geometry. The geometry of the identified architectural elements and their constituent facies are shown in table 2. Four small (c.1m) measured sections were taken in the Styrrup Quarry to show the heterogeneities within and across facies.

Table 2: Descriptions and interpretations of architectural elements at outcrop (after Wakefield et al., 2015).

Architectural elements in outcrops (Wakefield et al., 2015)	Facies association in cores (this study)	Constituent lithofacies (this study)	Geometry
Channel	Facies association 1	Gmg, Sp, Spmc, Sh, Sss, Sc, Fl	concave up (channelised)
Chute channel	Facies association 1	Gmg, Sp, Spmc, Sh, Sss, Sc, Fl	concave up (channelised)
Downstream accreting barforms	Facies association 2	Gmg, Sl, St, Sh, Fl	Lensoidal
Lateral accreting barforms	Facies association 2	Gmg, Sl, St, Sh, Fl	Lensoidal
Sandy floodplains	Facies association 3	Sh, Sss, Fl	Sheetlike

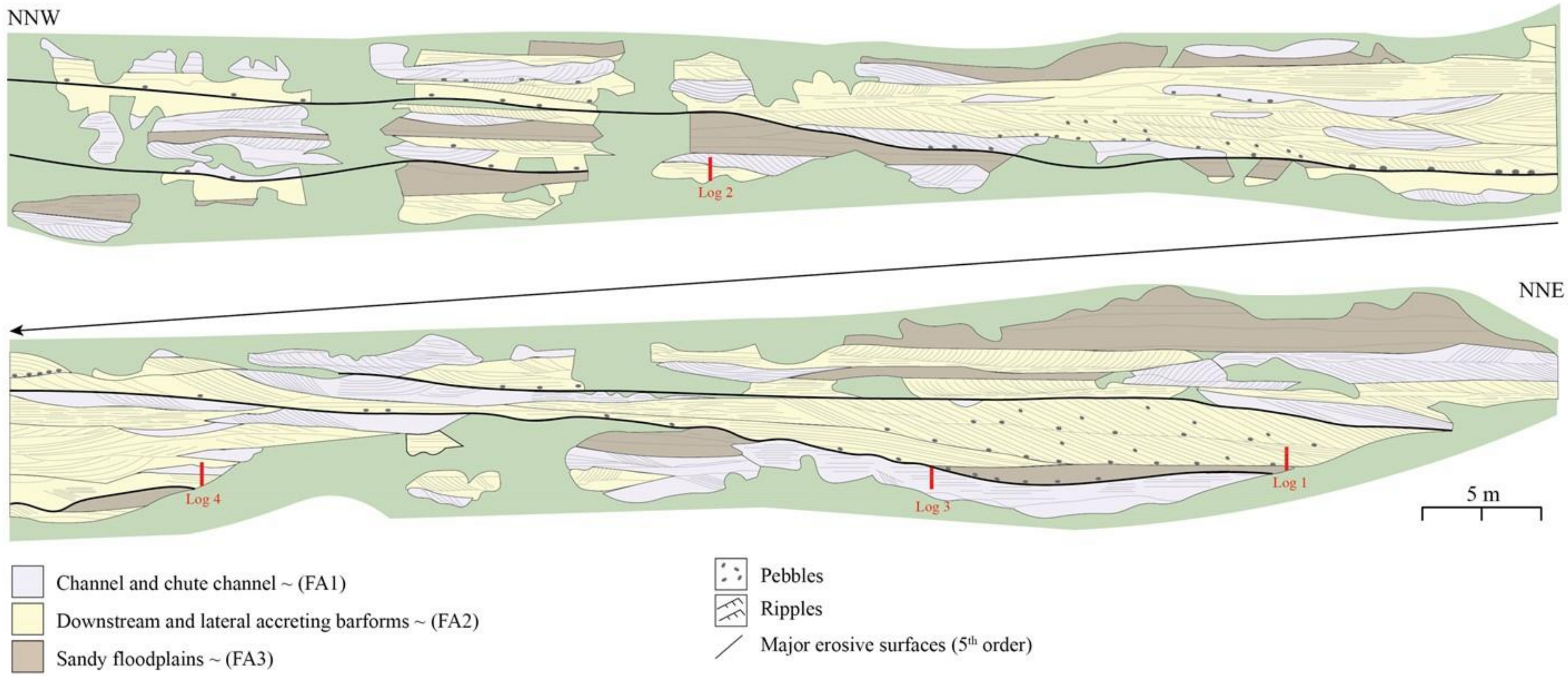

Figure 9: Architectural element panel for quarry face (represented by green color) in Styrrup Quarry (based on the original drawing published in Wakefield et al., 2015). Detailed sedimentary logs 1-4 that characterise lithofacies and facies associations are located. The bottom panel continues laterally from the top.

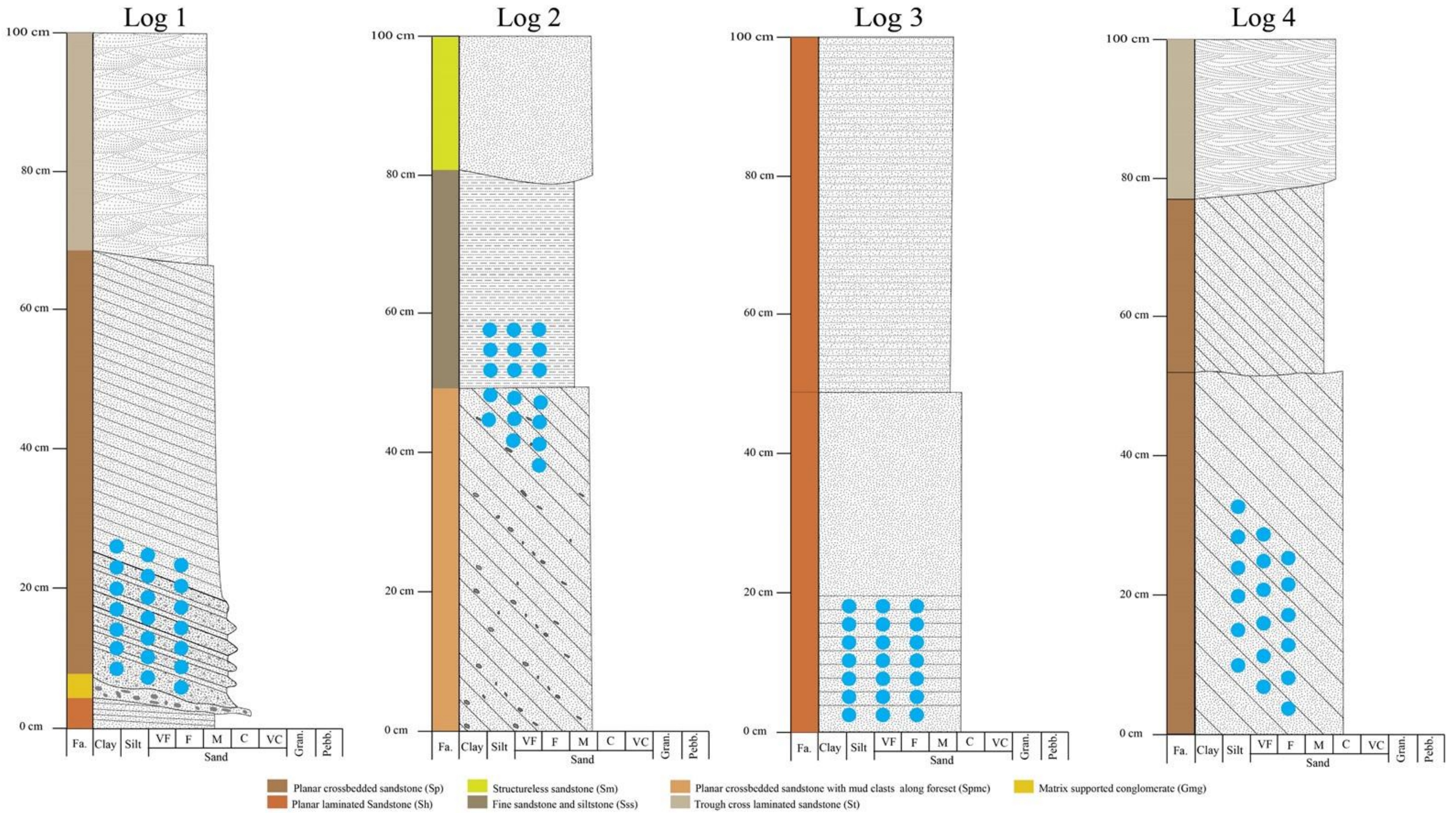

Figure 10: Small (c.1m) measured sections (Fig.9) in Styrrup Quarry showing lithological variation within individual facies and across facies boundaries. Blue circles show the points from where permeability measurements were taken.

4.4 Permeability distribution and variability

4.4.1 Core plug permeability

Permeability and porosity measurements from core plugs were previously conducted on samples obtained from the Endurance well 42/25d-3 at 1-foot (0.30-m) intervals (Weatherford, 2015). These values were then assigned to the interpreted lithofacies in the core log of the same well (Figs. 5-8). Crossplots of permeability versus helium porosity for lithofacies in each facies association are shown in Figure 11). At core plug scale, facies associations 1 and 2 have higher permeability than facies association 3. In comparison to facies association 1, facies association 2 has a more clearly defined cluster of high permeability facies and a smaller spread of data than facies association 1. Among the facies within these associations, planar and low angle cross-bedded sandstones (Sp, Sl) have relatively higher permeability than the trough cross-bedded sandstones (St) and planar cross-bedded sandstones with mudclasts along foresets (Spmc) (Fig. 11A, B). Structureless sandstones (Sm) have higher porosity and permeability than planar bedded sandstones (Sh) (Fig. 11A, B). Mottled and deformed sandstones (Smd) and crinkly laminated sandstones (Sc) have a wide range of porosity and permeability, reflecting the mixture of sandstone and mudstone that these facies contain (Fig. 11C). Mudstones (Fl) and matrix-supported conglomerates (Gmg) are the facies with lowest permeability (Fig. 11C).

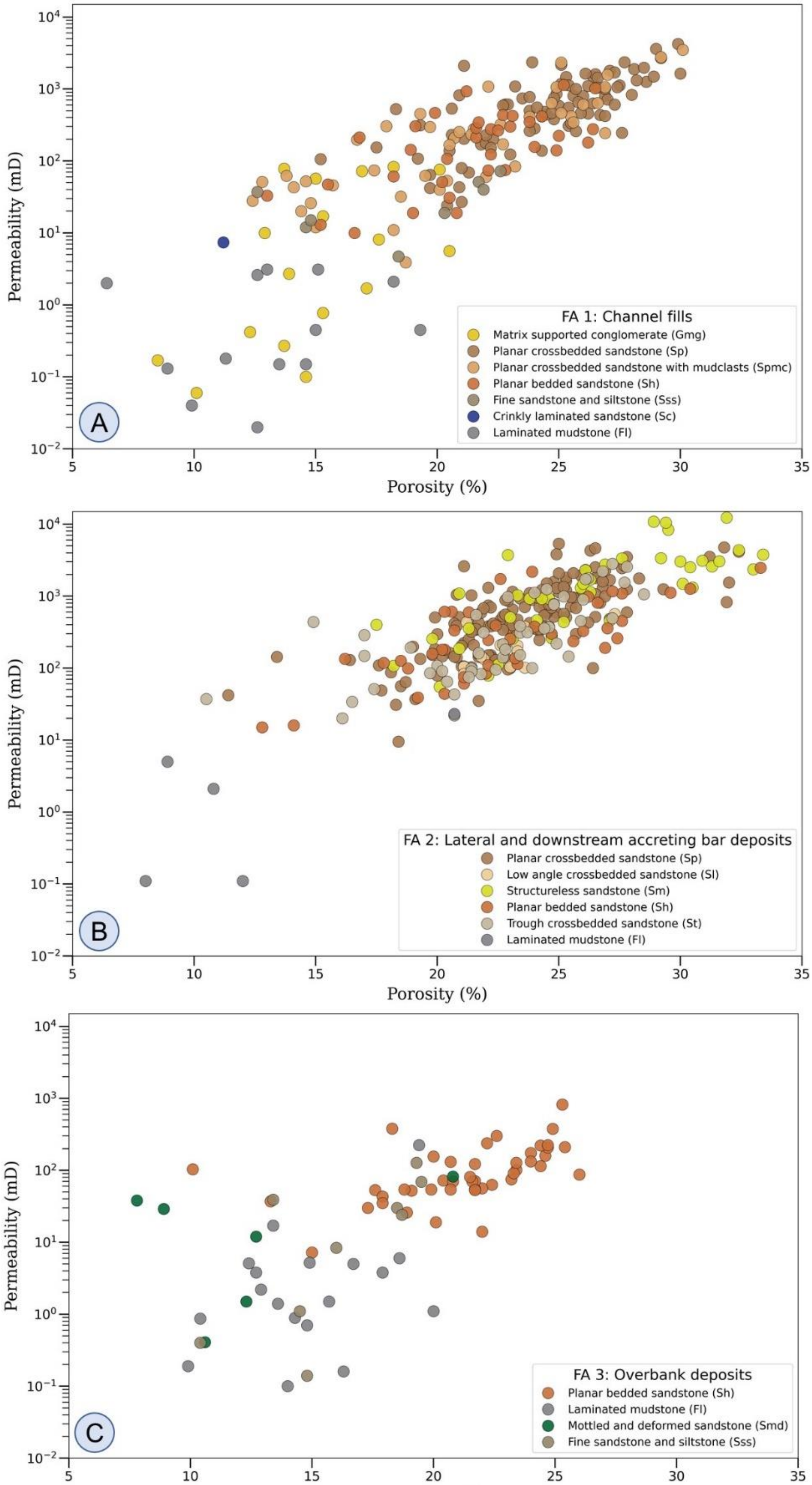

153 Figure 11: Core plug porosity and permeability distributions of different facies in three facies associations. A)
154 FA1, channel-fill deposits; B) FA2, lateral- and downstream-accreting bars; and C) FA3, overbank deposits.

4.4.2 Minipermeameter data

In the studied facies, core plug permeability data have an overall range of 0.02-12400 mD with a Q1 and Q3 value of 71 mD and 756 mD, respectively (Fig. 12). Corresponding permeability values for minipermeameter data range from 0.93-3930 mD with Q1 and Q3 values 109 mD and 748 mD respectively (Fig. 12). Permeability measurements from these two sources are therefore in relatively close agreement.

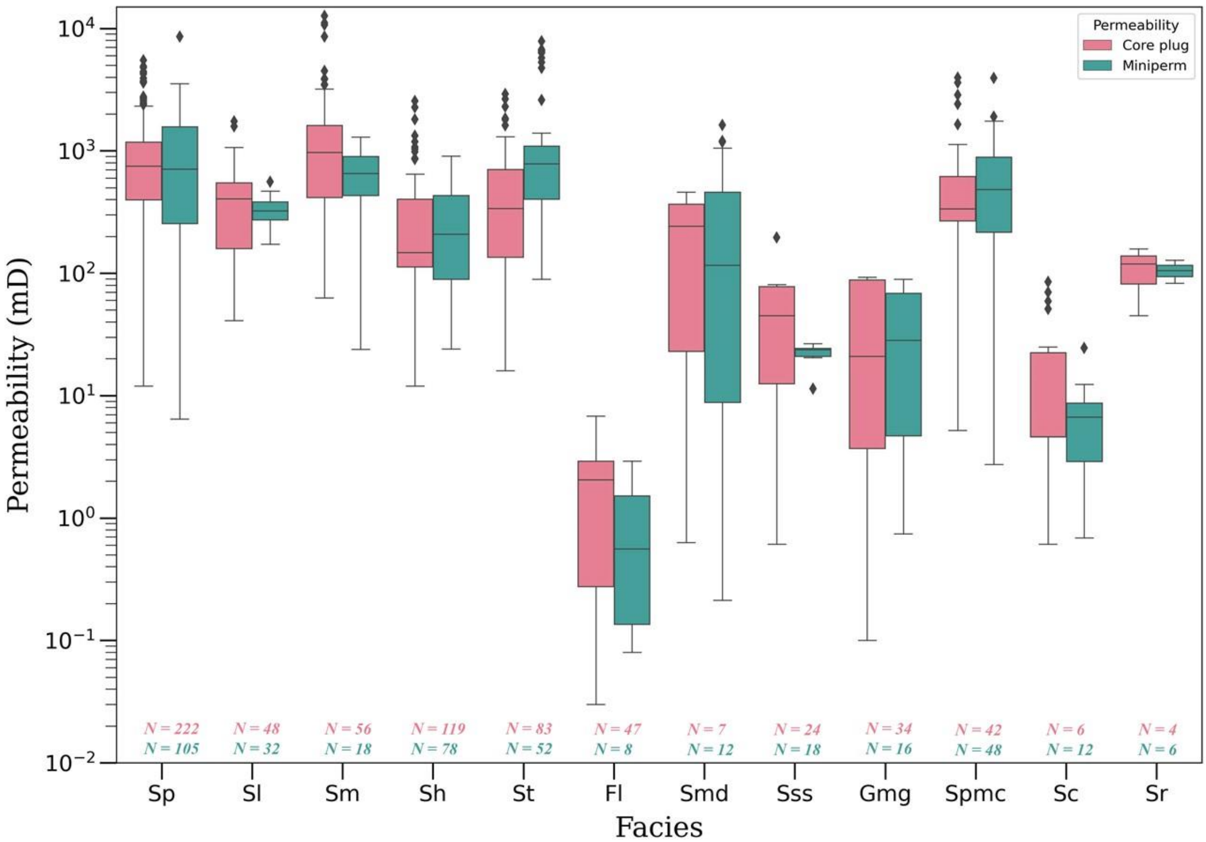

Figure 12: Box plot showing the range of permeability values for different facies from core plug and probe permeability measurements in well 42/25d-3. The number of measurements is also shown in the plot.

Among the core facies, structureless sandstones (Sm) and cross-bedded sandstones (Sp, Spmc, St) have high median permeability values. Permeability in facies Sp ranges from 9.5-5350 mD (median of 826 mD) in the core plugs and 23-2230 mD (median of 701 mD) in the minipermeameter measurements. Permeability in facies St and Sl ranges from 13-2810 mD and 35-1670 mD in the core plugs and the minipermeameter measurements range from 12-1780 mD and 124-1570 mD, respectively. Median permeability values of these facies are 427 mD and 482 mD in core plugs, and 411 mD and 560 mD in the minipermeameter measurements, respectively.

Planar cross-bedded sandstones with mudclasts along foresets (Spmc) exhibit a relatively larger range of permeability values than other cross-bedded sandstones (Sp, St). Permeability values of the former facies range from 4-3850 mD and 114-3930 mD in core plug and minipermeameter data, respectively with median value of 566 mD. Parallel laminated sandstone (Sh) has lower permeability than the cross bedded and structureless sandstones, with median Values of 292 mD in core plugs and 398 mD in minipermeameter measurements. Fine sandstone and siltstone (Sss) has a median permeability of 24 mD. Mottled and deformed sandstone facies (Smd) and crinkly laminated sandstone (Sc) show variable permeability due to the presence of muddy layers and the sand filled desiccation cracks. Matrix supported conglomerate (Gmg) and laminated mudstone (Fl) have the lowest median permeability values, of 1.6 mD and 0.65 mD, respectively. For all lithofacies, there is good agreement between minipermeameter and core plug permeability. Miniperm data of the same facies were also collected at the Styrrup Quarry. Similar variations were observed but the absolute values are higher (McKinley et al., 2011; McKinley et al., 2013) due to the friable nature of the rocks, hence they were not reported in this paper.

4.5 Facies heterogeneity and its influence on permeability

Along with the variation between facies, permeability variations within each facies has also been observed.

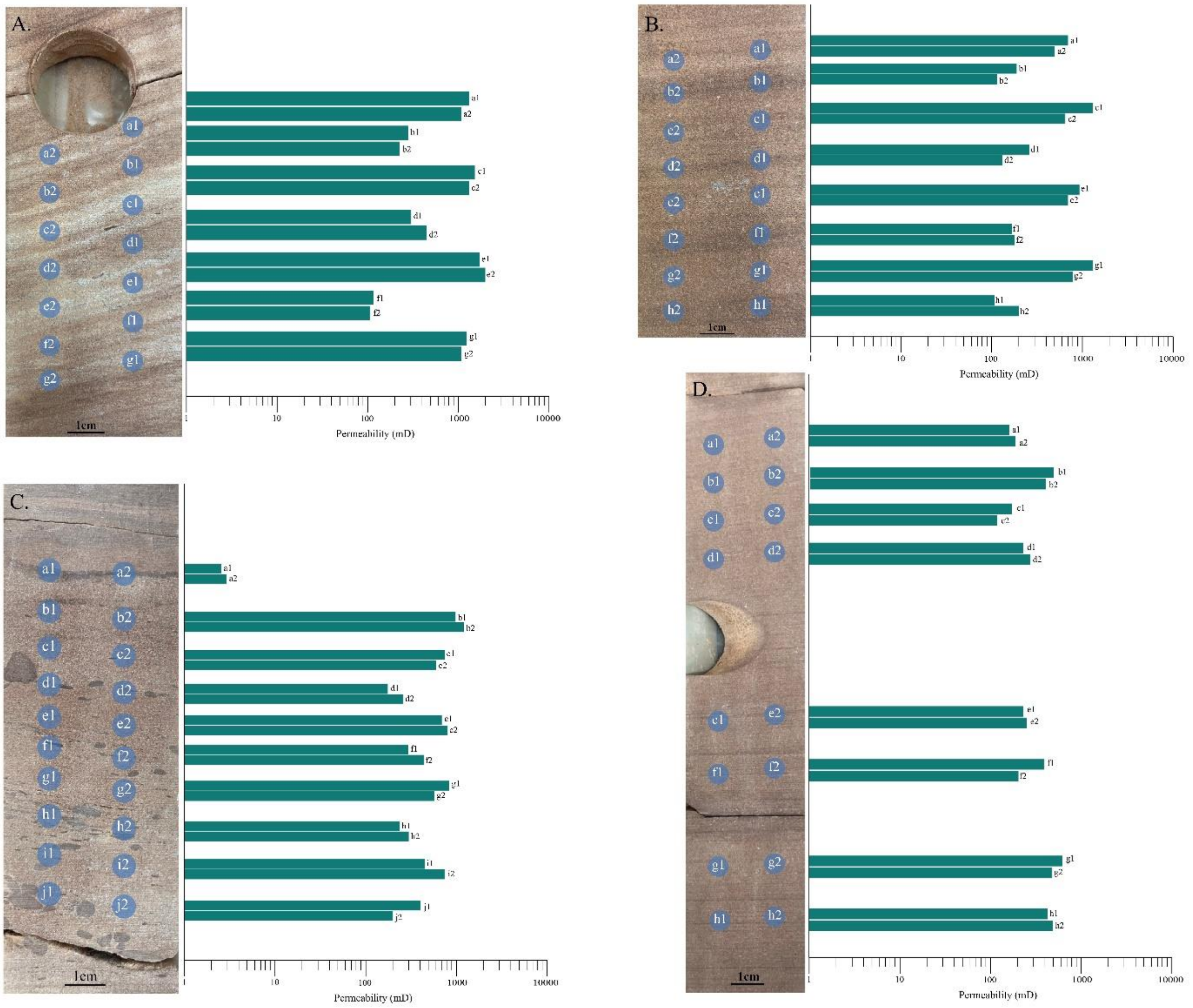

Figure 13: Lamina-scale permeability variations in cross-bedded sandstone facies: A) Sp; B) St; C) Spmc; and D) Sl.

In the cross-bedded sandstone facies, lamina-scale variations in permeability reflect alternating clay-rich and clay-poor laminae. Permeability varies between these laminae types by a factor of 5 in facies Sp and St, with clay-poor and clay-rich laminae exhibiting permeability values of c. 1000 mD and c. 200 mD, respectively (Fig. 13A, B). Permeability values vary by a factor of 4 in facies Spmc, with low values associated with mudclasts (Fig. 13C). Parallel laminated sandstones (Sh) also show internal variations in permeability between clay-rich (c. 200 mD) and clay-poor (c. 1000 mD) laminae (Fig. 14).

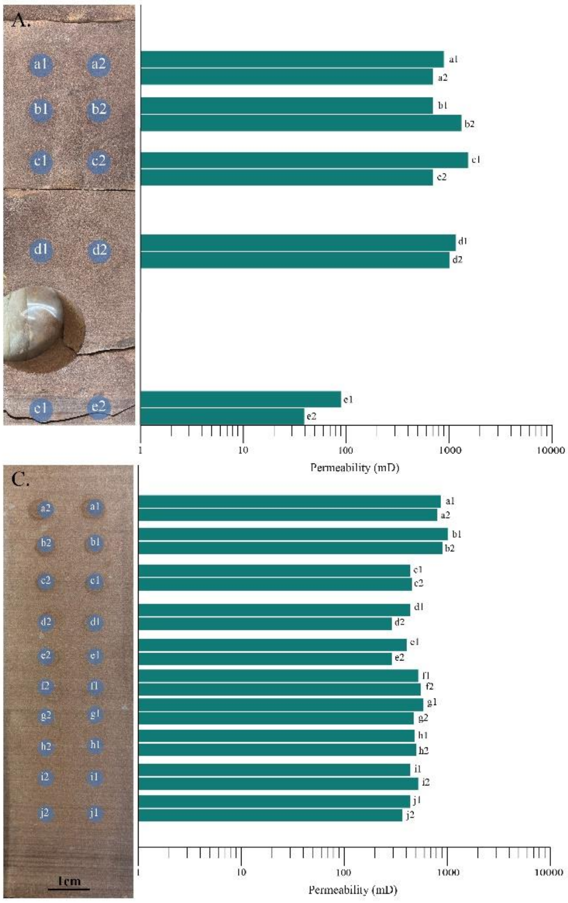

Figure 14: Lamina-scale permeability variations in sandstone facies that are not cross-bedded: A) Sm; B) Sh; and C) Sss.

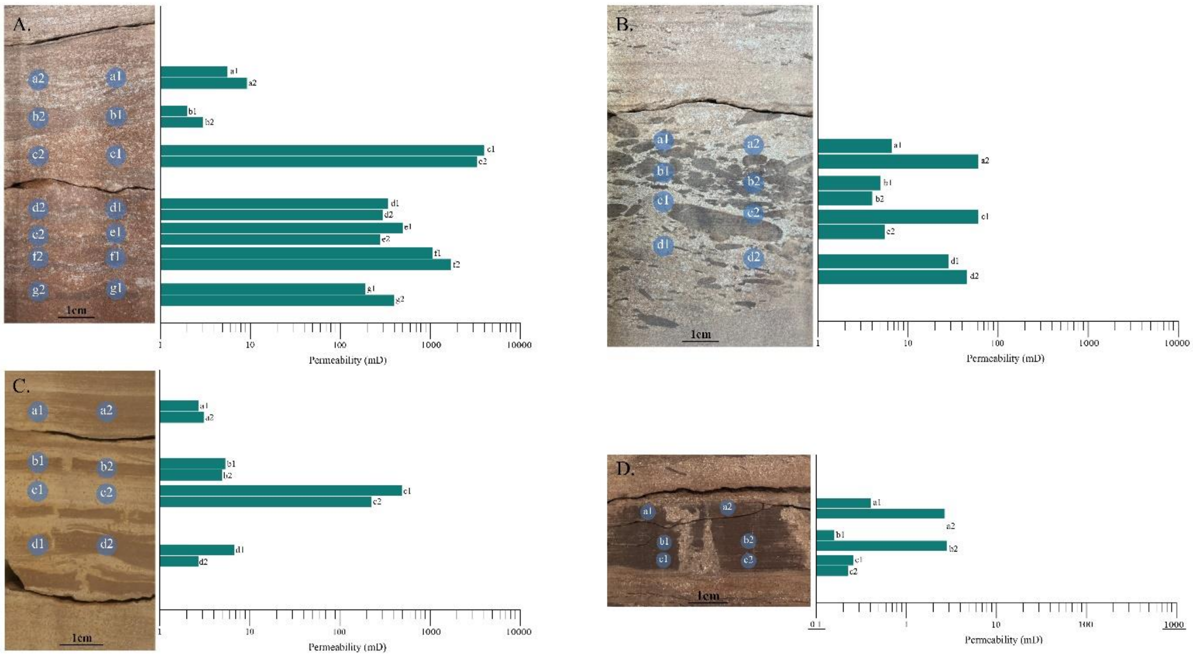

Figure 15: Lamina-scale permeability variations in conglomeratic and heterolithic sandstone facies: A) Sc; B) Gmg; C) Smd; and D) Fl. The permeability scale for facies Fl is different to that for other facies.

The sand filled desiccation cracks in Smd show higher permeability than the host muddy lithologies. Permeability of this facies range from as low as 2.8 mD in the muds to 48 mD in the sand. Matrix supported conglomerates (Gmg) also show variations of up to a factor of 4 (Fig.15), but the overall permeability of this facies and the mudstones are low. Permeability in the Gmg and Fl ranges from 0.79 -89 and 0.18-2.92 mD respectively.

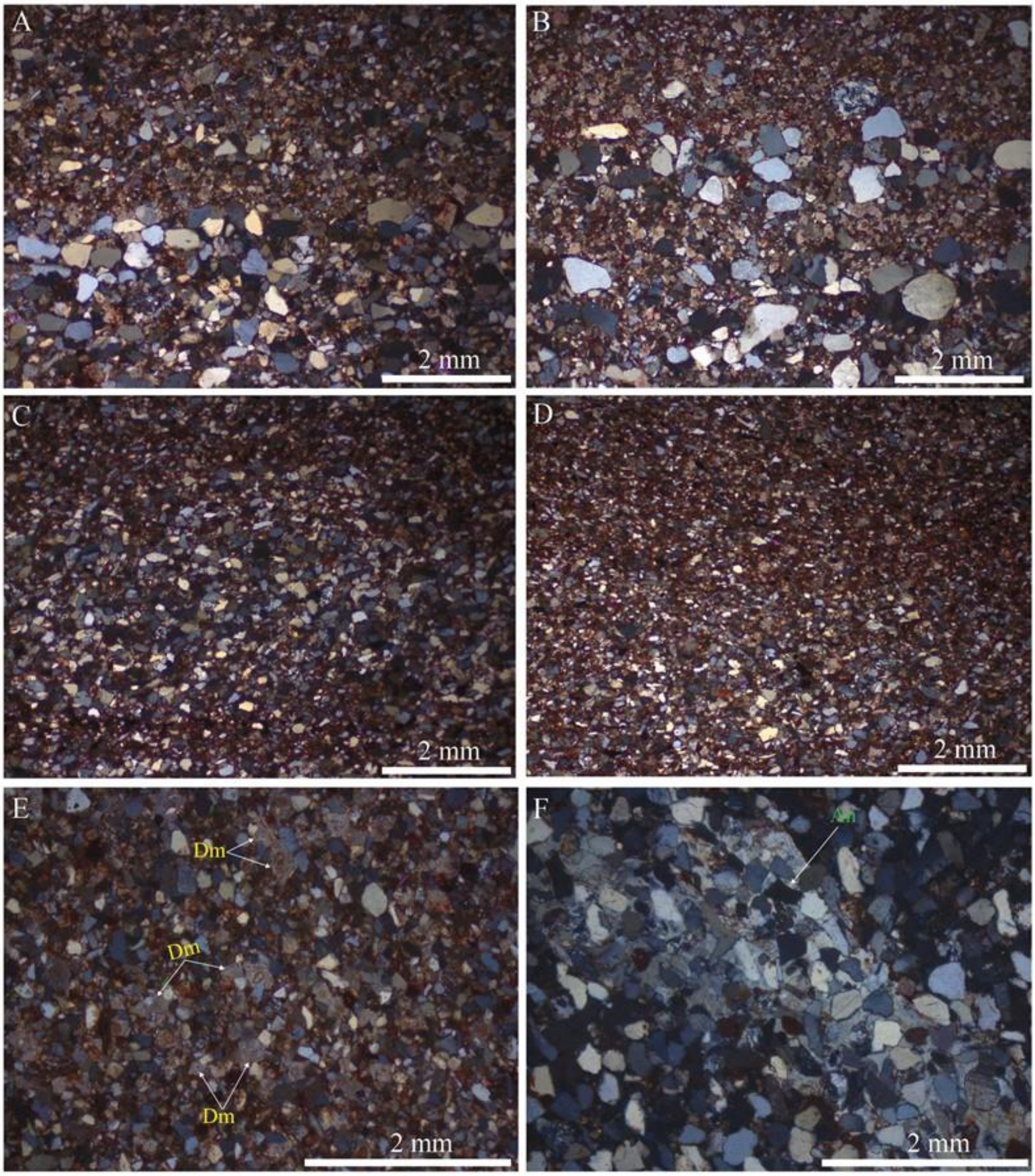

Figure 16: Photomicrographs showing alternating fine and medium grained laminae in: A, B) facies Sp; C) facies Sh; and D) St. Presence of: E) dolomite; and F) anhydrite cements was observed in facies Sp, St, and Sh.

Thin sections show that grain sizes are not uniform between sandstone facies. Cross-bedded and structureless sandstone facies (Sp, Spmc, St, Sl, and Sm) (Fig. 16A, 16B) are coarser grained than planar-bedded sandstones (Sh) (Fig. 16C). It is also evident that clay-rich laminae are finer-grained than clay-poor laminae in cross-bedded sandstone facies (Fig. 16A). The coarser grains are medium sand and the finer fraction are fine sand with clay minerals. Toeset laminae in the trough cross-bedded sandstone are finer grained than foreset laminae (Fig. 16D). In facies Sp, St, Spmc, coarser grains are surrounded by finer-grained matrix or dolomite cement (Fig. 16E, 16F). All of these lamina-scale and grain-scale heterogeneities are interpreted to contribute to permeability variations within facies (Payton et al., 2022).

5 Discussion

In the studied cores and outcrops, thirteen lithofacies are identified in the Bunter Sandstone Formation, typical of fluvial deposits. In the East Irish Sea basin aeolian facies have been reported in the Bunter Sandstone Formation and the equivalent formations (Cowan, 1993). But in the endurance field aeolian facies are missing. The most abundant of them are the facies that form accreting bar deposits (Medici et al., 2015).

Analysis of Bunter Sandstone Formation cores and outcrop analogue indicates that heterogeneities occur at multiple scales. The smallest scale heterogeneities observed in thin section, core and outcrop are laminae (e.g., alternating clay-poor and clay-rich foreset laminae in cross-bed sets). The thickness of the foreset laminae ranges from 1-1.5 cm. The next scale (10’s cm – 1’s m) of heterogeneity corresponds to sedimentary structures that define the internal architecture of lithofacies in core and outcrop. The stacking of lithofacies to form facies associations and architectural elements describes the third scale (1’s to 100’s m) of heterogeneity considered in this study (Fig. 9). Architectural elements correspond to units of a particular facies association, and can be distinguished at outcrop, where 2D and 3D geometrical relationships can be observed (e.g., at Styrrup Quarry), but not in 1D core. Facies associations provide a link between core and outcrop datasets in this context. The spatial distribution and interfingering of facies associations at this scale may control the distribution of high permeability sandstones.

Permeability variations in core plugs and minipermeameter measurements from core and outcrop occur over 3 orders of magnitude (Figs. 11-12), while permeability variations within facies are generally more subdued to less than 1 order of magnitude, (Figs. 13-15) but can reach 2 orders of magnitude, e.g., in facies Sp (Fig. 13A). These variations are controlled by the grain size and cement distribution. Permeability variations within facies also tend to occur along horizontal laminae (Sh) or along inclined foreset laminae in cross-bed sets (Sp, St, Spmc, and Sl). These lamina-scale permeability variations are likely to control the ratio of vertical to horizontal permeability, one of the main parameters that control residual saturation and fluid distributions in the subsurface (England et al., 1987; Dekker & Abriola, 2000), and may contribute to gravitational, capillary, and dissolution trapping (Dai et al., 2019).

5.1 Implications for trapping of CO_2

Numerical simulation studies show that fluid flow in homogeneous reservoirs is mainly controlled by buoyancy (Krishnamurthy et al., 2022). However, flow is dispersed by heterogeneity, which may enhance CO_2 trapping. CO_2 may thus occupy a larger pore volume in heterogeneous reservoirs, which will also reduce the column height of the buoyant CO_2 and decrease the chance of top-seal failure. Core flooding experiments show that heterogeneities can increase residual trapping by 3-5 times as a result of these mechanisms (Krevor et al., 2011). Krishnamurthy et al. (2017) showed that capillary pressure contrasts due to cm- to -m scale heterogeneities can affect the flow path of CO_2 and contribute to trapping capacity. Different sedimentary structures have different trapping potential owing to the geometry and lateral continuity of their internal laminae and beds. Cross-bedded facies are inherently more heterogeneous than their planar bedded counterparts due to their more complex stratification styles (Mishra & Haese, 2020). Topset and bottomset laminae in cross-bedded units are often less permeable than foreset laminae, consistent with our observations of the Bunter Sandstone Formation, and may therefore baffle CO_2 migration and disperse the CO_2 plume. Hollinsworth et al., (2024) identified and correlated laterally extensive mudstone layers and halite-cemented intervals in the Bunter Sandstone Formation, forming baffles that may help CO_2 to disperse laterally and increase residual trapping (Baz et al., 2016; Mishra & Haese, 2018).

5.2 Applicability at storage-unit and storage-complex scale

The findings of this study clearly show that sedimentological heterogeneity at lamina- to facies-scales causes significant variations in permeability. However, the effects of such heterogeneity are commonly omitted from numerical models built to estimate the total storage capacity and storage efficiency of CO_2 (Heinemann et al., 2012; Noy et al., 2012; Williams et al., 2013; Agada et al., 2017). Robust assessment of the effects of lamina- to facies-scales heterogeneity will require multiscale modelling (Aarnes et al., 2007; Ringrose et al., 2008; Nordahl et al., 2014; Milad et al., 2020). The first step in this approach will be to build small scale 3D models in order to derive effective properties that can be implemented in larger scale models, with models constructed at a hierarchy of scales that reflect the 3D organization of sedimentological heterogeneity.

6 Conclusions

This study investigated permeability variations in the Bunter Sandstone in relation to sedimentological heterogeneity through core and outcrop analysis, permeability measurements, and thin section analysis. A total of 13 lithofacies were identified with 12 of them present in the cores and 8 in the outcrop. There are three distinct facies associations identified in the cores, which are correlated with architectural elements identified in the outcrop of Bunter Sandstone Formation in Styrrup Quarry. Five architectural elements previously reported in the literature have been regrouped into three to match the core facies associations. Measurements of permeability in cores using a minipermeameter and from core plugs show variations of the order of three among facies and a factor of five within individual facies. Cross-bedded and structureless sandstone facies (Sp, St, Sl, Sm) have higher permeabilities than planar bedded facies (Sh, Sss) and deformed sandstone facies (Smd). Matrix supported conglomerate (Gmg) and the laminated mudstone (Fl) have the lowest permeability. Due to the presence of alternating clay rich and clay poor laminae and pebbles along the foreset, cross-bedded sandstone facies show higher permeability variations than the others. These variations are related to the variations of lithology and cementation as seen in thin sections.

Acknowledgements

This research was supported by a Bangabandhu Overseas Scholarship awarded to Shakhawat Hossain by the University of Dhaka, Bangladesh. The authors are grateful to the British Geological Survey for providing access to core material from the Endurance reservoir.

References

Aarnes, J. E., Kippe, V., Lie, K.-A., & Rustad, A. B. (2007). Modelling of multiscale structures in flow simulations for petroleum reservoirs. *Geometric modelling, numerical simulation, optimization: applied mathematics at SINTEF*, 307-360.

Agada, S., Kolster, C., Williams, G., Vosper, H., MacDowell, N., & Krevor, S. (2017). Sensitivity analysis of the dynamic CO2 storage capacity estimate for the Bunter Sandstone of the UK southern North Sea. *Energy Procedia*, *114*, 4564-4570.

Agartan, E., Trevisan, L., Cihan, A., Birkholzer, J., Zhou, Q., & Illangasekare, T. H. (2015). Experimental study on effects of geologic heterogeneity in enhancing dissolution trapping of supercritical CO2. *Water Resources Research*, *51*, 1635-1648.

Alshakri, J., Hampson, G. J., Jacquemyn, C., Jackson, M. D., Petrovskyy, D., Geiger, S., . . . Costa Sousa, M. (2023). A screening assessment of the impact of sedimentological heterogeneity on CO2 migration and stratigraphic-baffling potential: Sherwood and Bunter sandstones, UK. *Geological Society, London, Special Publications*, *528*, 245-266.

Ambrose, W., Lakshminarasimhan, S., Holtz, M., Núñez-López, V., Hovorka, S. D., & Duncan, I. (2008). Geologic factors controlling CO2 storage capacity and permanence: case studies based on experience with heterogeneity in oil and gas reservoirs applied to CO2 storage. *Environmental Geology*, *54*, 1619-1633.

Arts, R., Vandeweijer, V., Hofstee, C., Pluymaekers, M., Loeve, D., Kopp, A., & Plug, W. (2012). The feasibility of CO2 storage in the depleted P18-4 gas field offshore the Netherlands (the ROAD project). *International Journal of Greenhouse Gas Control*, *11*, S10-S20.

Bachu, S., & Adams, J. (2003). Sequestration of CO2 in geological media in response to climate change: capacity of deep saline aquifers to sequester CO2 in solution. *Energy Conversion management*, *44*, 3151-3175.

Baz, H., Noureldin, M., Allinson, W., & Cinar, Y. (2016). A field-scale investigation of residual and dissolution trapping of CO2 in a saline formation in Western Australia. *International Journal of Greenhouse Gas Control*, *46*, 86-99.

Bryant, S. L., Lakshminarasimhan, S., & Pope, G. A. (2008). Buoyancy-dominated multiphase flow and its effect on geological sequestration of CO2. *SPE Journal*, *13*, 447-454.

Cameron, T. D. J., Crosby, A., Balson, P. S., Jeffery, D. H., G.K., L., Bulat, J., & Harrison, D. J. (1992). United Kingdom offshore regional report: the geology of the southern North Sea. *HMSO, London*.

Chen, H., Wilson, S., & Monger-McClure, T. (1999). Determination of relative permeability and recovery for North Sea gas-condensate reservoirs. *SPE Reservoir Evaluation Engineering*, *2*, 393-402.

Cheng, A. H. D. (1984). Darcy's flow with variable permeability: A boundary integral solution. *Water Resources Research*, *20*, 980-984.

Corbett, P., Ringrose, P., Jensen, J., & Sorbie, K. (1992). Laminated clastic reservoirs: The interplay of capillary pressure and sedimentary architecture. SPE Annual Technical Conference and Exhibition?,

Cowan, G. (1993). Identification and significance of aeolian deposits within the dominantly fluvial Sherwood Sandstone Group of the East Irish Sea Basin UK. *Geological Society, London, Special Publications*, *73*, 231-245.

Dai, Z., Viswanathan, H., Xiao, T., Hakala, A., Lopano, C., Guthrie, G., & McPherson, B. (2019). Reactive transport modeling of geological carbon storage associated with CO2 and brine leakage. In *Science of Carbon Storage in Deep Saline Formations* (pp. 89-116). Elsevier.

Dekker, T. J., & Abriola, L. M. (2000). The influence of field-scale heterogeneity on the infiltration and entrapment of dense nonaqueous phase liquids in saturated formations. *Journal of Contaminant Hydrology*, *42*, 187-218.

England, W., Mackenzie, A., Mann, D., & Quigley, T. (1987). The movement and entrapment of petroleum fluids in the subsurface. *Journal of the Geological Society*, *144*, 327-347.

Farajzadeh, R., Zitha, P. L., & Bruining, H. (2009). Enhanced mass transfer of CO2 into water: experiment and modeling. SPE Europec featured at EAGE Conference and Exhibition?,

Fisher, J., Nichols, G., & Waltham, D. (2007). Unconfined flow deposits in distal sectors of fluvial distributary systems: examples from the Miocene Luna and Huesca Systems, northern Spain. *Sedimentary Geology*, *195*, 55-73.

Freeze, R. A., & Witherspoon, P. (1967). Theoretical analysis of regional groundwater flow: 2. Effect of water-table configuration and subsurface permeability variation. *Water Resources Research*, *3*, 623-634.

Gao, H., & Li, H. A. (2016). Pore structure characterization, permeability evaluation and enhanced gas recovery techniques of tight gas sandstones. *Journal of Natural Gas Science Engineering*, *28*, 536-547.

Gershenzon, N. I., Ritzi Jr, R. W., Dominic, D. F., Mehnert, E., & Okwen, R. T. (2017). Capillary trapping of CO2 in heterogeneous reservoirs during the injection period. *International Journal of Greenhouse Gas Control*, *59*, 13-23.

Ghazi, S., & Mountney, N. P. (2009). Facies and architectural element analysis of a meandering fluvial succession: The Permian Warchha Sandstone, Salt Range, Pakistan. *Sedimentary Geology*, *221*, 99-126.

Gibling, M. R. (2006). Width and thickness of fluvial channel bodies and valley fills in the geological record: a literature compilation and classification. *Journal of sedimentary Research*, *76*, 731-770.

Gluyas, J. G., & Bagudu, U. (2020). The Endurance CO2 storage site, blocks 42/25 and 43/21, UK North Sea. *Geological Society of London Memoirs*, *52*, 163-171.

Gotkowitz, M. (1993). *A study of the relationship between permeability distributions and small scale sedimentary features in a fluvial formation*.

Grenfell, M. (2012). Chute channnels in large, sand-bed meandering rivers. In: UK.

Heinemann, N., Wilkinson, M., Pickup, G. E., Haszeldine, R. S., & Cutler, N. A. (2012). CO2 storage in the offshore UK Bunter Sandstone Formation. *International Journal of Greenhouse Gas Control*, *6*, 210-219.

Hoegh-Guldberg, O., Jacob, D., Bindi, M., Brown, S., Camilloni, I., Diedhiou, A., . . . Guiot. (2018). Impacts of 1.5 C global warming on natural and human systems.

Hollinsworth, A., de Jonge-Anderson, I., Underhill, J., & Jamieson, R. (2024). Impact of reservoir quality on the carbon storage potential of the Bunter Sandstone Formation, southern North Sea. *Geoenergy*, *2*, geoenergy2023-2037.

Honarpour, M., Cullick, A., Saad, N., & Humphreys, N. (1995). Effect of rock heterogeneity on relative permeability: implications for scale-up. *Journal of Petroleum Technology*, *47*, 980-986.

Honarpour, M., & Saad, N. (1994). Influence of small-scale rock laminations on core plug oil/water relative permeability and capillary pressure. SPE University of Tulsa Centennial Petroleum Engineering Symposium,

Huysmans, M., Peeters, L., Moermans, G., & Dassargues, A. (2008). Relating small-scale sedimentary structures and permeability in a cross-bedded aquifer. *Journal of Hydrology*, *361*, 41-51.

Jones, M. W., Peters, G. P., Gasser, T., Andrew, R. M., Schwingshackl, C., Gütschow, J., Houghton, R.A, Friedlingstein, P., Pongratz, J., & Le Quéré, C. (2023). National contributions to climate change due to historical emissions of carbon dioxide, methane, and nitrous oxide since 1850. *Scientific Data*, *10*, 155.

Keller, C., Van Der Kamp, G., & Cherry, J. (1988). Hydrogeology of two Saskatchewan tills, I. Fractures, bulk permeability, and spatial variability of downward flow. *Journal of Hydrology*, *101*, 97-121.

Kovscek, A. R. (2002). Screening criteria for CO2 storage in oil reservoirs. *Petroleum Science Technology*, *20*, 841-866.

Krevor, S., Blunt, M. J., Benson, S. M., Pentland, C. H., Reynolds, C., Al-Menhali, A., & Niu, B. (2015). Capillary trapping for geologic carbon dioxide storage–From pore scale physics to field scale implications. *International Journal of Greenhouse Gas Control*, *40*, 221-237.

Krevor, S. C., Pini, R., Li, B., & Benson, S. M. (2011). Capillary heterogeneity trapping of CO2 in a sandstone rock at reservoir conditions. *Geophysical Research Letters*, *38*(15).

Krishnamurthy, P. G., DiCarlo, D., & Meckel, T. (2022). Geologic Heterogeneity Controls on Trapping and Migration of CO2. *Geophysical Research Letters*, *49*, e2022GL099104.

Krishnamurthy, P. G., Trevisan, L., & Meckel, T. (2017). Understanding the effects small scale heterogeneity on buoyancy driven CO2 migration for capillary trapped storage capacity estimation. *Energy Procedia*, *114*, 4954-4960.

Lewin, J., & Ashworth, P. J. (2014). The negative relief of large river floodplains. *Earth-Science Reviews*, *129*, 1-23.

Lewis, J. (1988). Outcrop-derived quantitative models of permeability heterogeneity for genetically different sand bodies. SPE Annual Technical Conference and Exhibition?,

Li, B., & Benson, S. M. (2015). Influence of small-scale heterogeneity on upward CO2 plume migration in storage aquifers. *Advances in water resources*, *83*, 389-404.

McKinley, J., Ruffell, A., & Worden, R. (2013). An integrated stratigraphic, petrophysical, geochemical and geostatistical approach to the understanding of burial diagenesis: Triassic Sherwood Sandstone Group, South Yorkshire, UK. *Linking Diagenesis to Sequence Stratigraphy*, 231-255.

McKinley, J. M., Atkinson, P. M., Lloyd, C. D., Ruffell, A. H., & Worden, R. (2011). How porosity and permeability vary spatially with grain size, sorting, cement volume, and mineral dissolution in fluvial Triassic sandstones: the value of geostatistics and local regression. *Journal of sedimentary Research*, *81*, 844-858.

Medici, G., Boulesteix, K., Mountney, N., West, L., & Odling, N. (2015). Palaeoenvironment of braided fluvial systems in different tectonic realms of the Triassic Sherwood Sandstone Group, UK. *Sedimentary Geology*, *329*, 188-210.

Miall, A. D. (1977). Lithofacies types and vertical profile models in braided river deposits: a summary.

Milad, B., Ghosh, S., Slatt, R., Marfurt, K., & Fahes, M. J. E. (2020). Practical aspects of upscaling geocellular geological models for reservoir fluid flow simulations: A case study in integrating geology, geophysics, and petroleum engineering multiscale data from the Hunton Group. *13*, 1604.

Mishra, A., & Haese, R. (2018). Determining conditions of CO2 entry into intraformational baffles: A prerequisite to estimate residually trapped CO2 at reservoir scale. 14th Greenhouse Gas Control Technologies Conference Melbourne,

Mishra, A., & Haese, R. R. (2020). Quantification of the turning point saturation for cross bedded CO2 storage reservoirs. *International Journal of Greenhouse Gas Control*, *103*, 103185.

Neuzil, C. E. (1986). Groundwater flow in low-permeability environments. *Water Resources Research*, *22*, 1163-1195.

Nordahl, K., Messina, C., Berland, H., Rustad, A. B., & Rimstad, E. J. G. S., London, Special Publications. (2014). Impact of multiscale modelling on predicted porosity and permeability distributions in the fluvial deposits of the Upper Lunde Member (Snorre Field, Norwegian Continental Shelf). *387*, 85-109.

Noy, D., Holloway, S., Chadwick, R., Williams, J., Hannis, S., & Lahann, R. (2012). Modelling large-scale carbon dioxide injection into the Bunter Sandstone in the UK Southern North Sea. *International Journal of Greenhouse Gas Control*, *9*, 220-233.

Pantou, I. (2014). Impact of stratigraphic heterogeneity on hydrocarbon recovery in carbonate reservoirs: Effect of karst.

Payton, R. L., Chiarella, D., & Kingdon, A. J. S. R. (2022). The influence of grain shape and size on the relationship between porosity and permeability in sandstone: A digital approach. *12*, 7531.

Petrovskyy, D., Jacquemyn, C., Geiger, S., Jackson, M. D., Hampson, G. J., Machado Silva, J. D., Judice, S., Rahman, F., & Costa Sousa, M. (2023). Rapid flow diagnostics for prototyping of reservoir concepts and models for subsurface CO2 storage. *International Journal of Greenhouse Gas Control*, *124*, 103855.

Picard, M. D., & High, L. R. (1973). *Sedimentary structures of ephemeral streams*. Elsevier.

Porada, H., Ghergut, J., & Bouougri, E. H. (2008). Kinneyia-type wrinkle structures—critical review and model of formation. *Palaios*, *23*(2), 65-77.

Possemiers, M., Huysmans, M., Peeters, L., Batelaan, O., & Dassargues, A. (2012). Relationship between sedimentary features and permeability at different scales in the Brussels Sands. *Geologica Belgica*.

Prosser, D., McKeever, M., Hogg, A., & Hurst, A. (1995). Permeability heterogeneity within massive Jurassic submarine fan sandstones from the Miller Field, northern North Sea, UK. *Geological Society, London, Special Publications*, *94*, 201-219.

Rashid, B., Muggeridge, A., Bal, A., & Williams, G. (2012). Quantifying the impact of permeability heterogeneity on secondary-recovery performance. *SPE Journal*, *17*, 455-468.

Ringrose, P., Nordahl, K., & Wen, R. (2005). Vertical permeability estimation in heterolithic tidal deltaic sandstones. *Petroleum Geoscience*, *11*, 29-36.

Ringrose, P., Pickup, G., Jensen, J., Forrester, M., Schatzinger, R. A., & Jordan, J. F. (1999). The Ardross Reservoir Gridblock Analog: Sedimentology, Statistical Representivity, and Flow Upscaling. In *Reservoir Characterization—Recent Advances* (Vol. 71, pp. 0). American Association of Petroleum Geologists. https://doi.org/10.1306/m711c18

Ringrose, P. S., Martinius, A. W., & Alvestad, J. J. G. S., London, Special Publications. (2008). Multiscale geological reservoir modelling in practice. *309*, 123-134.

Stalkup, F., & Ebanks, W. (1986). Permeability variation in a sandstone barrier island-tidal channel-tidal delta complex, Ferron Sandstone (Lower Cretaceous), central Utah. SPE Annual Technical Conference and Exhibition,

Stephen, K. D., Clark, J. D., & Gardiner, A. R. (2001). Outcrop-based stochastic modelling of turbidite amalgamation and its effects on hydrocarbon recovery. *Petroleum Geoscience*, *7*, 163-172.

Trevisan, L., Cihan, A., Fagerlund, F., Agartan, E., Mori, H., Birkholzer, J. T., Zhou, G., & Illangasekare, T. H. (2014). Investigation of mechanisms of supercritical CO2 trapping in deep saline reservoirs using surrogate fluids at ambient laboratory conditions. *International Journal of Greenhouse Gas Control*, *29*, 35-49.

Trevisan, L., Krishnamurthy, P., & Meckel, T. A. (2017). Impact of 3D capillary heterogeneity and bedform architecture at the sub-meter scale on CO2 saturation for buoyant flow in clastic aquifers. *International Journal of Greenhouse Gas Control*, *56*, 237-249.

Trevisan, L., Pini, R., Cihan, A., Birkholzer, J. T., Zhou, Q., & Illangasekare, T. H. (2015). Experimental analysis of spatial correlation effects on capillary trapping of supercritical CO 2 at the intermediate laboratory scale in heterogeneous porous media. *Water Resources Research*, *51*, 8791-8805.

Wakefield, O. J., Hough, E., & Peatfield, A. W. (2015). Architectural analysis of a Triassic fluvial system: the Sherwood Sandstone of the East Midlands Shelf, UK. *Sedimentary Geology*, *327*, 1-13.

Weatherford. (2015). Conventional Core Analysis [Report]. 1-519.

Williams, J., Jin, M., Bentham, M., Pickup, G. E., Hannis, S., & Mackay, E. J. (2013). Modelling carbon dioxide storage within closed structures in the UK Bunter Sandstone Formation. *International Journal of Greenhouse Gas Control*, *18*, 38-50.

Ziegler, P. A. J. (1982). Geological atlas of western and central Europe.